Congruent population genetic structures and divergence histories in anther-smut fungi and their host plants *Silene italica* and the *S. nutans* species complex

Running title:

Co-structure of anther-smuts and their hosts

Fanny E. Hartmann[1], Alodie Snirc[1], Amandine Cornille[2], Cécile Godé[3], Pascal Touzet[3], Fabienne Van Rossum[4,5], Elisabeth Fournier[6], Stéphanie Le Prieur[1], Jacqui Shykoff[1], Tatiana Giraud[1]

[1] Ecologie Systematique Evolution, Batiment 360, Universite Paris-Saclay, CNRS, AgroParisTech, 91400 Orsay, France;

[2] Genetique Quantitative et Evolution–Le Moulon, INRAE, Universite Paris-Saclay, CNRS, AgroParisTech, 91198 Gif-sur-Yvette, France;

[3] Univ. Lille, CNRS, UMR 8198 - Evo-Eco-Paleo, F-59000 Lille, France;

[4] Meise Botanic Garden, B-1860 Meise, Belgium;

[5] Fédération Wallonie–Bruxelles, B-1080 Brussels, Belgium;

[6] UMR BGPI, Univ. Montpellier, INRA, CIRAD, Montpellier SupAgro, Montpellier, France;

[*] Author for Correspondence: Fanny E. Hartmann, Ecologie Systematique Evolution, Batiment 360, Universite Paris-Saclay, CNRS, AgroParisTech, 91400 Orsay, France, phone number : 01 69 15 72 82, e-mail address: fanny.hartmann@u-psud.fr

Abstract

The study of population genetic structure congruence between hosts and pathogens gives important insights into their shared phylogeographic and coevolutionary histories. We studied the population genetic structure of castrating anther-smut fungi (*Microbotryum* genus) and of their host plants, the *Silene nutans* species complex, and the morphologically and genetically close *S. italica,* which can be found in sympatry. Phylogeographic population genetic structure related to persistence in separate glacial refugia has been recently revealed in the *S. nutans* plant species complex across Western Europe, identifying several distinct lineages. We genotyped 171 associated plant-pathogen pairs of anther-smut fungi and their host plant individuals using microsatellite markers and plant chloroplastic SNPs. We found clear differentiation between fungal populations parasitizing *S. nutans* and *S. italica* plants. The population genetic structure of fungal strains parasitizing the *S. nutans* plant species complex mirrored the host plant genetic structure, suggesting that the pathogen was isolated in glacial refugia together with its host and/or that it has specialized on the plant genetic lineages. Using random forest approximate Bayesian computation (ABC-RF), we found that the divergence history of the fungal lineages on *S. nutans* was congruent with the one previously inferred for the host plant and likely occurred with ancient but no recent gene flow. Genome sequences confirmed the genetic structure and the absence of recent gene flow between fungal genetic lineages. Our analyses of host-pathogen individual pairs contribute to a better understanding of co-evolutionary histories between hosts and pathogens in natural ecosystems, in which such studies are still scarce.

Key words: population genetic structure, host-pathogen interaction, cryptic speciation, genetic divergence, approximate Bayesian computation, coevolution

Introduction

Host-pathogen interactions are pervasive in natural ecosystems, with many important ecological and evolutionary consequences (Poulin, 2005; Thompson, 2005). Pairs of tightly interacting hosts and pathogens may share common evolutionary histories due to co-evolution and/or shared geographic and climatic constraints, or may follow distinct evolutionary trajectories due to differences in reproductive systems, dispersal ranges, population sizes or contingent histories (Tellier, de Vienne, Giraud, Hood, & Refrégier, 2010; Thompson, 2005). The comparison of genetic divergence histories between host and pathogen populations gives important insights into their shared phylogeographic history and possible local adaptation or host specialization (Croll & Laine, 2016; Feurtey et al., 2016). Studies of phylogeny congruence of hosts and pathogens can for example allow identifying host shifts or co-speciation events (de Vienne et al., 2013; Hafner & Page, 1995; Wilson, Falush, & McVean, 2005). Several cases of host shift or co-speciation events between hosts and pathogens have led to damaging diseases in plants, animals and humans (Fisher, Gow, & Gurr, 2016; McDonald & Stukenbrock, 2016; Wolfe, Dunavan, & Diamond, 2007). The study of population genetic structure congruence within species or species complexes can help identifying and understanding patterns of local adaptation (Gandon, Capowiez, Dubois, Michalakis, & Olivieri, 1996), which play an important role in the dynamics of pathogen and host communities (Gandon & Michalakis, 2002; Laine, 2005; Laine, 2008). Studies investigating the congruence of population genetic structure and divergence histories between hosts and pathogens are yet surprisingly still scarce despite their importance for understanding the evolutionary mechanisms and histories leading to host specialization and local adaptation (Barrett, Thrall, Burdon, & Linde, 2008; Croll & Laine, 2016), but see (Dybdahl & Lively, 1996; Feurtey et al., 2016; McCoy, Boulinier, & Tirard, 2005; Michalakis, Sheppard, Noel, & Olivieri, 1993; Tsai &

70 Manos, 2010).

71 Anther-smut fungi (*Microbotryum* genus) are generally highly specialized on their host plant
72 species of the Caryophyllaceae family (Hartmann et al., 2019; Kemler, Göker, Oberwinkler, &
73 Begerow, 2006; Le Gac, Hood, Fournier, & Giraud, 2007; Refrégier et al., 2008) and patterns of
74 local adaptation have been reported in the system (Feurtey et al., 2016; Kaltz, Gandon,
75 Michalakis, & Shykoff, 1999). Therefore, they constitute a highly suitable system to study the
76 congruence of population genetic structure and divergence history between hosts and pathogens
77 at different evolutionary scales. Comparisons of phylogenies at the genus level suggested a
78 prevalence of host shifts at large evolutionary scales (Refrégier et al., 2008). The plant *Silene*
79 *latifolia* and its anther-smut fungus *M. lychnidis-dioicae* display strong congruence of population
80 genetic structures and plant local adaptation at regional and continental scales, suggesting the
81 existence of co-evolution in the system (Delmotte, Bucheli, & Shykoff, 1999; Feurtey et al.,
82 2016; Kaltz et al., 1999). Population genetic structures of both the host and the fungal pathogen
83 likely resulted from past climatic events, showing hallmarks of recolonization from former
84 glacial refugia in Europe (Badouin et al., 2017; Gladieux, Devier, Aguileta, Cruaud, & Giraud,
85 2013; Gladieux et al., 2011; Taylor & Keller, 2007; Vercken et al., 2010). The congruence of
86 host and pathogen population genetic structures has not been investigated in other anther-smut
87 fungi-*Silene* pairs despite their importance as models of pathosystems in natural ecosystems
88 (Bernasconi et al., 2009; Toh & Perlin, 2016) and the importance of assessing whether
89 congruence in population genetic subdivision is a general pattern (Croll & Laine, 2016).
90 Furthermore, the evolutionary history of population genetic divergence and of gene flow levels
91 occurring between pathogens infecting closely related hosts with overlapping distribution ranges
92 still remain poorly studied at the genome-wide-scale (but see Badouin et al., 2017).

93 *Silene nutans* is an assemblage of strongly differentiated cryptic genetic plant lineages,
94 corresponding to at least seven "evolutionary significant units", which can be grouped into two
95 main phylogeographic (eastern and western) genetic clusters in Europe (Van Rossum et al.,
96 2018). The *S. nutans* genetic lineages display several morphological and ecological differences,
97 as well as nuclear and plastid genetic differentiation (Martin et al., 2016; Van Rossum et al.,
98 2018), and strong postzygotic reproductive isolation has been shown between the eastern and
99 western clusters in Western Europe (Martin et al., 2017). Geographic distribution patterns suggest
100 that *S. nutans* lineages have diverged in allopatry during the Quaternary climate oscillations, and
101 then recolonized northwards, without admixture (Martin et al., 2016; Martin et al., 2017; Van
102 Rossum et al., 2018). The anther-smut fungal species *Microbotryum violaceum sensu stricto* is
103 specialized on *S. nutans* (Kemler et al., 2006; Lutz et al., 2005). *Microbotryum* fungi are
104 pollinator-borne pathogens castrating plants by replacing the pollen by their own spores and
105 aborting ovaries, and they are usually highly specific on their *Silene* host plant species (Le Gac,
106 Hood, & Giraud, 2007; Refrégier et al., 2008). The existence of cryptic lineages within *S. nutans*
107 therefore raises the question of whether cryptic lineages also exist in the fungus and whether their
108 genetic divergence history mirrors that of the host. In Southern Europe, *S. nutans* can be found in
109 sympatry with *S. italica*, a closely related species, in particular in the Cévennes (Lafuma &
110 Maurice, 2006). *Silene nutans* and *S. italica* can be difficult to distinguish, being very similar
111 morphologically, mainly differing in petal shape, in the length of the gynophore and with rather
112 nodding or erect flowers, respectively (Rameau, Mansion, & Dumé, 1989, 2008; Tison & de
113 Foucault, 2014). Their flowering time, pollinator guilds and ecological niches overlap, although
114 they slightly differ in their ecological requirements, with *S. italica* being strictly calcicolous,
115 more xero-thermophilous and heliophilous than *S. nutans* (Rameau et al., 1989, 2008; Tutin et al.,
116 2001). *Microbotryum* fungi have been found on the two plant species and appeared differentiated

117 based on a small sample and a few genetic markers (Bucheli, Gautschi, & Shykoff, 2000);
118 however, spillover, i.e., non-sustainable cross-species disease transmission, has been shown to
119 occur in *Microbotryum* fungi (Antonovics, Hood, & Partain, 2002; Gladieux et al., 2011). The
120 study of the population genetic structure of *M. violaceum s. s.* on *S. nutans* therefore requires
121 molecular typing to check plant and fungal species identities.

122 In this study, we analyzed associated plant-pathogen samples of *S. nutans* and *S. italica*
123 populations from Europe in order to address the following questions: 1) Is there genetic
124 differentiation between anther-smut fungi parasitizing the closely related plant species *S. nutans*
125 and *S. italica*? Are there hybrids and/or spill-overs in anther-smut fungi? 2) Is the population
126 genetic structure of the anther-smut fungi parasitizing *S. nutans* and *S. italica* congruent with
127 those of their hosts? 3) What is the divergence history of these anther-smut fungi on their hosts?
128 Did genetic divergence occur with gene flow? Does the divergence history of the fungi mirror
129 that of their hosts? In order to address these questions, we used genetic markers (nuclear
130 microsatellite markers and/or chloroplastic SNPs) in both plants and anther-smut fungi to analyse
131 diseased material (171 plant-pathogen pairs) collected across Western Europe and infer
132 population genetic structures. We used approximate Bayesian computation (ABC) to compare
133 genetic divergence scenarios in anther-smut fungi in order to assess whether the genetic
134 divergence history in anther-smut fungi mirrored that inferred previously for their host plants. We
135 also sequenced 53 genomes of *Microbotryum* fungi and analysed them together with 46 available
136 *Microbotryum* genomes to assess whether the inferences on population genetic structure and gene
137 flow based on microsatellite markers hold at the genome-wide levels and whether there were
138 spill-overs or gene flow from other sympatric *Microbotryum* species than those analysed with
139 microsatellite markers.

Materials and Methods

Fungal and plant materials

We analyzed 171 anther-smut fungi collected from diseased plant individuals of *S. nutans* and *S. italica* that were sampled in 55 distinct geographic sites across Europe, including the United Kingdom, France, Belgium, Switzerland, Italy, Germany and Norway (Table S1, Fig. 1A). Diseased plant individuals were stored in individual paper envelopes kept in plastic bags filled with silica gel, in dark conditions at 8°C. Small pieces of leaves were used as raw material for DNA extraction of host plant individuals. Diploid spores of *Microbotryum* anther-smut fungi were collected in buds of infected flowers and grown as yeasts on potato dextrose agar (PDA) medium, and then stored at -20°C. Spores did not grow for a few samples older than two years. For DNA extraction of these strains, we used the dried spores directly collected from anthers of diseased flowers. In most cases, spores from anthers of a single flower were used and therefore corresponded to a single *Microbotryum* genotype (López-Villavicencio et al., 2007). When spore material was limited, we used multiple anthers from several flowers of the same plant. We never observed more than two alleles per strain and found low levels of heterozygosity per strain, indicating that we unlikely genotyped more than one fungal genotype.

Genotyping and identification of species and genetic lineages of the *Silene* plants based on nuclear microsatellite markers and chloroplastic SNPs

We extracted plant DNA of at least one diseased plant individual per site using the NucleoSpin® 96 Plant II kit (Macherey-Nagel, Germany). We obtained DNA for 134 out of the 171 diseased

plant individuals. At least one host individual was genotyped per site, except for six sites due to the lack of plant material (Table S1). In addition, we genotyped three plant individuals for which no anther-smut fungus was isolated but strains were isolated at the same sites (sample # 874_4, 874_6, 512_3). Using morphological criteria of the host plant species, sample collectors initially identified 153 *S. nutans* and 18 *S. italica* diseased individuals. However, as the morphologies of *S. nutans* and *S. italica* are very similar, misidentification could occur. Therefore, we sequenced four chloroplast fragments (*psbA*, *LF*, *MATK*, *GS*; Lahiani et al., 2013) to check species identity of the diseased plants collected in southeastern France and in Italy, where both *S. nutans* and *S. italica* can be found. We thus reassigned one individual to *S. nutans* and seven individuals to *S. italica,* while one host individual could not be assigned to either *S. nutans* or *S. italica* species (from the pair # 1436). We excluded this host-pathogen individual pair from our analyses. We thus had 145 diseased *S. nutans* plants and 25 diseased *S. italica* plant (Table S1).

To further genotype the plant individuals for studying the population genetic structure, we used a combination of plastid (chloroplast) SNPs and nuclear microsatellite markers as previously described (Godé et al., 2014; Martin et al., 2016; Martin et al., 2017). For plastid markers, using the KASPAR® protocol we genotyped six SNPs, named Cp42, Cp397, Cp540, Cp656, Cp730 and Cp804, and polymorphic for [T/G], [A/C], [C/T], [G/T], [C/T], and [T/G], respectively. Individual haplotypes were defined as combinations of allelic states for all six SNPs. For nuclear markers, we used six multiplexes genotyping 24 microsatellite markers (Table S2). We followed the previously published protocols (Godé et al., 2014; Martin et al., 2016; Martin et al., 2017), except that we used different dye colors, bought from Eurofins Genomics. We used the Multiplex PCR Kit (Qiagen) following manufacturer instructions for PCR reactions, performed separately for each multiplex in 15 µL volume containing 3 µL of DNA, 3.4 µL of H_2O, 7.1 µL of multiplex

PCR Kit (Buffer 2X, Qiagen, USA), and 1.4 µL of the primer mix. The primer mix included 2 µM of unlabelled forward and reverse primers and 0.5 µM or 0.75 µM of the labelled forward primer depending on the dye label. We used the same PCR cycling program as described in (Godé et al., 2014) with some modifications of the final elongation for multiplex 1 (Table S3A-C). We checked successful PCR amplifications on 2% (w/v) agarose gel electrophoresis. We outsourced genotyping at the Gentyane Genotyping Platform (INRA, Clermont, France) and scored alleles with GENEMAPPER v.4.0 (Applied Biosystems). We excluded three markers (SIL18, SIL26, SIL42) for which we had less than 50% of the individuals successfully genotyped. Given the material available, we could genotype 136 host plant individuals using both plastid SNPs and nuclear microsatellite markers. All 136 genotyped host individuals had a determined plastid haplotype and a determined genotype for at least 50% of the 21 remaining nuclear microsatellite markers.

Genotyping and species identification of the *Microbotryum* fungal strains: microsatellite markers and ITS sequences

We extracted fungal DNA using the Chelex protocol (Biorad, USA) following (Giraud, 2004). We extracted DNA from the 170 strains of anther-smut fungi, either from mixes, stored at -20°C, of haploid sporidia resulting from clonal growth after meiosis or from diploid teliospores directly collected in anthers of diseased flowers and stored at 10°C. Diploid genomes were therefore genotyped. DNA was diluted half-fold for PCR amplification. We used the internal transcribed spacer (ITS) to check that the genus of the fungal strains belonged to the *Microbotryum* genus. To genotype the fungal strains, we used 22 microsatellite markers arranged into multiplex (Table S4 ; (Fortuna et al., 2016; Giraud et al., 2008)). We used the Multiplex PCR Kit (Qiagen) following manufacturer instructions for PCR reactions which were performed separately for each

multiplex as described above. We used the PCR cycling programs as in previous studies (Fortuna et al., 2016; Giraud et al., 2008; Table S3C-D). We checked the success of PCR amplifications on 2 % agarose gel electrophoresis. For genotyping, we pooled multiplexes 7 and 8 as a single multiplex. We outsourced genotyping at the Gentyane Genotyping Platform (INRA, Clermont, France) and scored alleles with GENEMAPPER v.4.0 (Applied Biosystems). We could determine the genotypes for all strains for at least 50% of the 22 markers. We identified 21 fungal strains that were likely siblings of other fungal strains based on null genetic distances and we excluded them from the STRUCTURE software analyses (Table S1; see below).

Population genetic structure based on microsatellite markers

To analyze and compare host and pathogen population genetic structures, we used a combination of three complementary approaches using microsatellite nuclear markers on both the *Silene* host plants and anther-smut fungal datasets. First, we used the model-based Bayesian clustering approach implemented in the software STRUCTURE version 2.3.4 (Pritchard, Stephens, & Donnelly, 2000). The program performs partitions of multilocus genotypes into genetic clusters and assigns individuals to genetic clusters, minimizing the departure from expected frequencies and linkage equilibrium among loci. We tested an admixture model with correlated frequencies and no prior information for K = 2 to K = 10 clusters. A total of 10 repetitions were run for each K value. We used 50,000 samples as a burn-in period and 100,000 samples per run for the Monte Carlo Markov Chain (MCMC) replicates. Cluster assignment probabilities were computed using the CLUMPP program (Jakobsson & Rosenberg, 2007) implemented in the R package {Pophelper}. We used the R package {Pophelper} (https://github.com/royfrancis/pophelper) to build the barplots. We choose as the biologically most relevant K value the finer population structure, as the highest K value for which a new cluster could be identified with individuals

highly assigned to it, the new cluster at {K+1} having only admixed individuals (i.e. mean membership coefficient <0.80 to the given cluster). For the anther-smut fungus dataset, genetic data were haploidized as individuals were highly homozygous. High homozygosity levels might bias inferences in the software STRUCTURE as these are based on Hardy-Weinberg expectations in a diploid setting (Pritchard et al., 2000). Furthermore, 21 strains were removed, appearing as siblings of other strains, with identical genotypes. *Microbotryum* fungi have one obligatory sexual event before plant infection, so that clonemates cannot be found in different plants, but high selfing rates may allow the same genotype to be found in neighbor plants if they are parasitized by the same diploid spores or offspring (Giraud, 2004). For the host plant dataset, genetic data were kept as diploid and five individuals were removed as they had identical genotypes as other neighbor plants and may be clonemates. We identified clonemates and siblings in both datasets using the dist(X) function in the R package {Ape} (Paradis, Claude, & Strimmer, 2004) and considered two individuals to be siblings if their distance was equal to 0. We then used two methods for assessing population genetic structure that do not assume outcrossing or a lack of linkage disequilibrium. We performed a discriminant analysis of principal components (DAPC) using the R package {ADEGENET} (Jombart, 2008; Jombart & Ahmed, 2011) and used a principal component analysis (PCA) with the dudi.pca function using the R package {ade4} (Dray & Dufour, 2007) on the entire set of individuals in both datasets. Maps showing genotypes per locality were drawn using the R package {maps} (Becker, Wilks, Brownrigg, Minka, & Deckmyn, 2017) and {mapplots} (Gerritsen, 2013). Scatter plots were performed using the R package {ggplot2} (Wickham, 2009).

Population statistics of genetic diversity and structure based on microsatellite markers

We computed, using the R package {diveRsity} (Keenan, McGinnity, Cross, Crozier, & Prodöhl,

2016), the following estimates of genetic diversity per locus, site, genetic cluster identified in the STRUCTURE analysis and/or species for the host plants and for the anther-smut fungi datasets: the number of alleles, allelic richness (A_R), observed heterozygosity (H_O), expected heterozygosity (H_E), the fixation indexes (F_{ST}, F_{IS} and F_{IT}), and the Jost's D statistics corresponding to the fraction of allelic variation found among genetic clusters. We tested whether genotype frequencies fitted the Hardy-Weinberg expectations using a standard Chi² goodness of fit method and assessed the significance of F_{ST}, F_{IS} and F_{IT} values using a bootstrap procedure with 1000 iterations and calculating 95% confidence intervals. Sites with less than three sampled individuals were pooled with other sites of the same genetic lineage when they were closer than 1/10th of latitude or longitude or were otherwise excluded from the analyses. We thus excluded nine sites for the plants (site # 1014, 303, 1532, 719, 1546, 1547, 1437, 429, 1548, 1438) and 13 sites for the fungal pathogens (site # 1068, 1014, 303, 1532, 719, 1546, 940, 1547, 1437, 333, 1249, 6809, 1548) as they contained too few samples for computing relevant population genetics statistics and were too far from other populations to be pooled with them. In total, we considered 20 groups of sites for the host and 19 groups of sites for the pathogen. We included sibling individuals but excluded individuals with admixed membership between genetic clusters inferred from the STRUCTURE analysis (i.e. individuals with mean membership coefficient <0.80 to the given cluster), which may be due to low assignment power or admixture. To take into account differences of sample size between sites, we also estimated allelic richness using ADZE (Szpiech, Jakobsson, & Rosenberg, 2008) which corrects for sample size difference. Calculations were performed using a standardized sample size of N=3, corresponding to the smallest number of observations per site. We tested for mean differences in diversity statistics between species and genetic clusters using a Wilcoxon rank sum test and a Kruskal-Wallis rank sum test in the R software v3.5.3, respectively, considering values across groups of sites. To study isolation-by-

distance patterns in the *S. nutans* and fungi parasitizing *S. nutans* datasets, we computed correlations between matrices of genetic and geographic distances of plant and fungal populations using a Mantel test. Genetic distances between populations at each group of sites were calculated as the Nei's distance (Nei, 1972) using the dist.genpop() function of the R package {ADEGENET} (Jombart, 2008; Jombart & Ahmed, 2011). Geographic distances were calculated using the distm() function of the R package{geosphere}. We computed Mantel tests using the mantel.rtest() function of the R package {ade4} with 1,000,000 resamples for the null distribution. We also studied the correlations between matrices of genetic distances of plant and fungal populations using a Mantel test as above. To remove the effect of the correlation between genetic and geographic distances in the correlation between matrices of genetic distances, we also performed a partial Mantel test using the partial.mantel.test() function of the R package {ncf} with 1,000,000 resamples for the null distribution (Feurtey et al., 2016). We considered 16 group of sites, the same both for the host and the pathogen, corresponding to *S. nutans* host plants and fungal strains belonging to the genetic cluster parasitizing S. *nutans.* We excluded sites of *S. italica* host plants and fungal strains belonging to the genetic cluster parasitizing *S. italica,* and one site studied in the host but not studied in the pathogen (site # 333). We investigated the occurrence of recent events of effective population size reduction (i.e. bottlenecks) within the identified fungal genetic clusters using the program BOTTLENECK version 1.2.02 (Piry, Luikart, & Cornuet, 1999).

Inference of anther-smut fungi divergence history based on microsatellite markers

We studied the divergence history of the anther-smut fungi sampled on the *S. nutans* lineage complex using an approximate Bayesian computation-random forest (ABC-RF) procedure that

performs ABC inferences based on the machine learning tool named "random forest" (Breiman, 2001; Pudlo et al., 2016; Raynal et al., 2019). The divergence history of the host had already been previously inferred (Martin et al., 2016; Martin et al., 2017; Van Rossum et al., 2018). To increase our power to disentangle between different evolutionary scenarios, we performed model choice and parameter estimation by comparing scenarios or groups of scenarios in sequential rounds, each round testing a particular type of evolutionary event, either divergence time, order of divergence or presence of gene flow (Estoup, Raynal, Verdu, & Marin, 2018; Liu et al., 2019); Table 1; Table S5). We built scenarios based on the genetic clusters obtained using microsatellite markers and on previous analyses of divergence of anther-smut fungi and their host species (Badouin et al., 2017; Gladieux et al., 2013; Martin et al., 2016; Martin et al., 2017; Van Rossum et al., 2018). The tested scenarios varied regarding the time of divergence, the relative order of divergence of fungal genetic clusters and the occurrence of gene flow among genetic fungal clusters (Table S5). We did not include scenarios with variation in effective population sizes as the BOTTLENECK analysis did not identify any signature of effective population size reduction (see 'Results' section). To test if the order of sequential rounds had an effect on the outcome of the analysis, we tested the time of divergence and the relative order of divergence as either the first or the second round (Note S1). We used as populations the fungal genetic clusters identified through population structure analyses and removed fungal strains that were likely siblings of other fungal strains in each genetic cluster.

We ran the ABC procedure modified from (Liu et al., 2019). Briefly, we simulated datasets with 22 fungal microsatellite markers using the ABCtoolbox program (Wegmann, Leuenberger, Neuenschwander, & Excoffier, 2010) and used fastsimcoal 2.5 for coalescent-based simulations (Excoffier & Foll, 2011). We simulated 10,000 genetic datasets per scenario using coalescent

simulations with model parameters drawn from prior distributions (Table S6A). We set prior distributions based on previous analyses of divergence of anther-smut fungi and of their host species (Badouin et al., 2017; Branco et al., 2018; Gladieux et al., 2013; Martin et al., 2016; Martin et al., 2017; Van Rossum et al., 2018). We set a generation time of one year for the pathogen based on its life cycle (Thrall, Biere, & Antonovics, 1993). We estimated the following parameters: effective size of each genetic cluster (*N*), divergence time and migration rate per generation between two genetic clusters *x* and *y* (*Txy* and *mxy*, respectively). We computed 16 summary statistics for the observed and simulated datasets with the program arlsumstats (Table S6B; (Excoffier & Lischer, 2010). We assumed a generalized stepwise model of microsatellite evolution (Estoup, Jarne, & Cornuet, 2002) and allowed the mutation rate to vary across microsatellite markers. We drew locus-specific mutation rates from a gamma distribution (α,α/μ) in which μ is the mutation rate per generation and α is a shape parameter (Cornille et al., 2012; Liu et al., 2019). We used the R package {abcrf} v1.7.0 (Pudlo et al., 2016) to compute a classification vote through ABC-RF, representing the number of times a scenario was selected among classification *n* trees of the constructed random forest. We chose n=500 trees. For each round, we selected the scenario or group of scenarios with the highest number of classification votes. We computed the posterior probability and the prior error rates over 10 replicated analyses. We performed a linear discriminant analysis (LDA) in the R package {abcrf} v1.7.0 (Pudlo et al., 2016) on the simulated and observed datasets to visually check the fit of the model to the observed data. Finally, we performed parameter inferences using the group of models eventually selected.

Sequencing data and genome assemblies

We performed whole-genome sequencing for 23 anther-smut fungal strains parasitizing *S. italica* and 30 strains parasitizing *S. nutans*. Out of these 53 strains, 38 strains belonged to the 170 host-pathogen pairs that were genotyped with microsatellite markers (Table S7). Due to limited fungal material, we sequenced six additional strains that were collected at our studied sites but not genotyped for microsatellite markers and nine additional strains collected at three new sites (Table S7). We extracted DNA from fresh spores stored at -20°C using the Nucleospin Soil Kit (Macherey-Nagel, Germany). Genomes were sequenced using Illumina 150 bp paired-end sequencing technology at 46X coverage on average. We also included outgroups using available whole-genome sequences of 56 anther-smut fungal strains parasitizing closely-related host species of *S. nutans* and *S. italica* occurring in the studied geographic range (Le Gac, Hood, Fournier, et al., 2007; Refrégier et al., 2008): 33 *M. lychnidis-dioicae* strains parasitizing *S. latifolia* (Badouin et al., 2017), 19 *M. silenes-dioicae* strains parasitizing *S. dioica* (Badouin et al., 2017) and four *M. violaceum* var *paradoxa* strains parasitizing *S. paradoxa* (Branco et al., 2018). We downloaded raw data publicly available from the NCBI Sequence Read Archive (SRA) under the BioProject IDs PRJNA295022 and PRJEB16741 (Table S7). We thus analysed a total of 109 *Microbotryum* genomes. For read mapping, we used as reference genome the high-quality haploid genome assembly of the MvSn-1249 *M. violaceum s. str.* strain corresponding to the a_2 mating type (collected on *S. nutans*) previously obtained with P6/C4 Pacific Biosciences SMRT technology and annotated for gene models (Branco et al., 2017). The MvSn-1249-A2 assembly was accessed from GenBank BioProject accession number PRJEB12080 (BioSample ID: SAMEA3706514, assembly: GCA_900014965).

Genome read mapping and variant calling procedure

We performed read mapping and SNP calling of the 109 analysed genomes against the MvSn-

1249-A2 genome as previously described (Branco et al., 2018; Hartmann, Rodríguez de la Vega, Brandenburg, Carpentier, & Giraud, 2018). First, we trimmed Illumina raw reads for sequence quality and removed adapter sequences using the software Cutadapt v1.8.3 (Martin, 2011) with the options: -q 10, 10; –minimum-length 50; -a AGATCGGAAGAGCACACGTCTGAACTCCAGTCAC; -AAGATCGGAAGAGCGTCGTGTAGGGAAAGAGTGTAGATCTCGGTGGTCGCCGTATT. We aligned trimmed reads using the short read aligner bowtie2 v2.1.0 (Langmead, Trapnell, Pop, & Salzberg, 2009) with the three following software options: –very-sensitive-local; –phred33; -X 1000. We removed PCR duplicates using the MarkDuplicates tool of Picard tools version 2.14.1 (http://broadinstitute.github.io/picard) and performed local realignment of mapped reads using the tools RealignerTargetCreator and IndelRealigner of the Genome Analysis Toolkit (GATK) version 3.8 (McKenna et al., 2010) to improve alignment accuracy in indel regions. Mean alignment rates to the reference genome ranged from 53 to 96% (Table S7). For SNP calling, we used GATK version 3.7 (McKenna et al., 2010) and ran HaplotypeCaller on each strain individually using a diploid mode. Then, we used GenotypeGVCFs on a merged gvcf variant file to perform joint variant calls. We filtered SNP calls for quality using VariantFiltration and following the GATK good practices for hard-filtering of variants (QUAL < 250; QD < 2; MQ < 30.0; -10.5 > MQRankSum > 10.5; -5 > ReadPosRankSum > 5; FS > 60; SOR > 3) and masked SNPs for repeats. We found 41 SNPs in the strain MvSn-1249-A2 (the very same fungal strain as the reference genome also sequenced with Illumina), indicating low rates of false positives in our SNP calling. We only kept bi-allelic SNPs with a high genotyping rate (> 90%) on autosomes (i.e., excluding SNPs on the mating-type contigs MvSn-1249-A2-R1_MC15 and MvSn-1249-A2-R1_MC16). We excluded SNPs on the mating-type chromosomes for population genomics analyses as they exhibit suppressed recombination on 90% of their lengths (Branco et al., 2018).

399 Removing the strain MvSn-1249-A2, we kept 108 fungal strains and 1,305,369 SNPs for
400 population genomic analyses.
401
402 **Population genomics analyses**
403 To analyze the population genetic structures of anther-smut fungi parasitizing several *Silene*
404 species using the genome-wide SNP dataset called on autosomes, we used the model-based
405 Bayesian clustering approach implemented in the software STRUCTURE version 2.3.4
406 (Pritchard et al., 2000), from K=2 to K=10 clusters, and performed a PCA, similarly as for the
407 microsatellite datasets. For the STRUCTURE analysis, we selected a set of 233 unlinked SNPs
408 randomly distributed at intervals of 100 kb along the autosomes, linkage disequilibrium decaying
409 over 50-100 kb in *Microbotryum* populations (Badouin et al., 2017). We used the R package
410 {Pophelper} (https://github.com/royfrancis/pophelper) to perform barplots. We performed the
411 PCA on all SNPs (but excluding missing data and heterozygote genotypes) using the --pca
412 command of the Plink v1.9 software (Chang et al., 2015; Purcell et al., 2007). To study footprints
413 of gene flow between fungal strains, we performed a phylogenetic network analysis implemented
414 in splitsTree (Huson, 1998; Huson & Bryant, 2006) with the neighbornet method.
415
416 **Results**
417 **Population genetic structure and diversity of *Silene nutans* and *S. italica* host plants**
418 After checking plant species identity with molecular markers, we retained 145 diseased *S. nutans*
419 plants and 25 diseased *S. italica* plants (Table S1; Fig 1A). The 21 plant nuclear microsatellite
420 markers distinguished well *S. nutans* and *S. italica* both in STRUCTURE analyses from K=2 and

421 in the principal component analysis (PCA; Fig 1B-C; Fig S1).

422 Within *S. nutans*, we identified four distinct haplotypes based on the six plastid SNPs, retrieving
423 in our sample the four major genetic lineages of *S. nutans* previously identified in Western
424 Europe (Fig 1A; (Martin et al., 2016; Martin et al., 2017; Van Rossum et al., 2018). The blue,
425 yellow, orange, and red haplotypes were found, as in previous studies, in the northeastern,
426 southeastern, western and southwestern parts of Europe, respectively. All *S. italica* samples had a
427 blue plastid haplotype (Fig 1A). Within *S. nutans,* the PCA based on the 21 plant nuclear
428 microsatellite markers mainly differentiated the orange genetic lineage from the other ones (Fig
429 1B; Fig S1B) and the STRUCTURE analysis detected four genetic clusters, corresponding to the
430 different plastid haplotypes, except for the red haplotype for which we had too few samples (Fig
431 1C; Fig S1A). The STRUCTURE analysis further identified two well-separated genetic clusters
432 within the *S. nutans* orange plastid haplotype (Fig. 1C). These two genetic clusters also appeared
433 separated on the second axis of the PCA and corresponded to plant individuals collected in the
434 Northern part of France *versus* Belgium and Western part of France (Fig S1), in agreement with
435 previous findings (Martin et al., 2016). From the STRUCTURE analyses, we identified five host
436 individuals with admixed cluster memberships (mean membership coefficient <0.80 to the given
437 cluster), which may be due to low assignment power or admixture between genetic clusters. We
438 found no further clear subdivision within *S. nutans* at higher K values and no clear population
439 subdivision within *S. italica* (Fig S1A).

440 We found no significant differences in allelic richness neither between *S. nutans* and *S. italica*
441 (Wilcoxon rank sum (WRS) test on 20 groups of sites, W = 12, p-value = 0.169; Table S8A) nor
442 between the four *S. nutans* genetic clusters (Kruskal-Wallis rank sum (KWRS) test on 16 groups
443 of sites, $Chi^2 = 4.92$, degree of freedom (df) = 3, p-value = 0.178; Table S8A). In *S. nutans,* levels

444 of observed heterozygosity were significantly lower than those of expected heterozygosity under
445 Hardy-Weinberg equilibrium for most loci, the mean F_{IS} value per marker being 0.33 (Table S2).
446 In *S. italica,* levels of observed and expected heterozygosities were not significantly different for
447 most markers (78%; Table S2), the mean F_{IS} value per locus being 0.37 (Table S2). As expected,
448 pairwise F_{ST} and Jost's D indicated higher divergence between *S. italica* and *S. nutans* (mean
449 F_{ST}=0.32; mean Jost's D=0.57; Table S9A) than between genetic clusters of *S. nutans* (mean
450 F_{ST}=0.20; mean Jost's D=0.35; Table S9A; KWRS test for both statistics, W = 0, p-value =
451 0.010). For *S. nutans,* we found on average lower pairwise F_{ST} and Jost's D values between the
452 yellow Western cluster and the two orange Western and Northwestern genetic clusters (mean
453 F_{ST}=0.17; mean Jost's D=0.28; Table S9A) than between the blue Eastern genetic cluster and the
454 Western genetic clusters (mean F_{ST}=0.24; mean Jost's D=0.42; Table S9A), although the
455 difference was not significant (KWRS test for F_{ST}, W = 8, p-value = 0.200; KWRS test for Jost's
456 D, W = 9, p-value = 0.100). The correlation between the matrices of pairwise genetic and
457 geographic distances for *S. nutans* (tested on 16 sites) was significantly positive (Mantel test: r =
458 0.54, p-value < 0.001), indicating an isolation-by-distance pattern.

459

460 **Differentiation between anther-smut fungi parasitizing *Silene nutans* and *S. italica***

461 Population genetic structure analyses separated *Microbotryum* strains into two main genetic
462 clusters, corresponding to their host plant of sampling, *S. italica* and *S. nutans*. The host of
463 collection separated strains according to the first axis of the PCA (Fig 2B). The STRUCTURE
464 analysis and the discriminant analysis of principal component (DAPC) also delimitated two clear
465 fungal genetic clusters according to the host of sampling at K=2 (Fig 2C; Fig S2). In the PCA

(Fig. 2B), four *Microbotryum* strains sampled on *S. nutans* clustered with strains parasitizing *S. italica* and one *Microbotryum* strain sampled on *S. italica* clustered with strains parasitizing *S. nutans*. These strains may correspond to spill-overs, i.e. cross-species disease transmissions, between the two studied *Silene* species or from other *Silene* species. We excluded for further analyses the 11 strains that had their main cluster memberships < 80% in the STRUCTURE analysis at K=2 (Fig 2C), which can be due to low assignment power or admixture.

Anther-smut fungi parasitizing *S. italica* had on average higher levels of allelic richness (WRS test on 19 groups of sites, W = 48, p-value = 0.004) and observed heterozygosity (WRS test on 19 groups of sites, W = 30, p-value = 0.014) than anther-smut fungi parasitizing *S. nutans* (Table S8B). Levels of observed heterozygosity were significantly lower than heterozygosity expected under Hardy-Weinberg equilibrium for eight markers for *Microbotryum* fungi parasitizing *S. nutans* and six markers for *Microbotryum* fungi parasitizing *S. italica* (Table S4).

Similar genetic structure in anther-smut fungi as in their *Silene nutans* and *S. italica* host plants

The existence of additional levels of population genetic structure within fungal strains was indicated by the STRUCTURE barplots (Fig S2), the second and third principal components of the PCA that explained 27.9 % of the total variance between strains (Fig 2B). To investigate the population structure within each of the two main genetic clusters of anther-smut fungi, corresponding mainly to populations parasitizing *S. nutans* and *S. italica*, respectively, we analyzed them separately, which confirmed the existence of a strong population structure within anther-smut fungi parasitizing *S. nutans* (Fig 3A). The first two PCA axes separated fungal

strains into three distinct genetic clusters, corresponding to the three most frequent plastid haplotypes identified in the host plant (Fig 3A), which was also supported by the DAPC and the STRUCTURE analyses (Fig 3B; Fig S3). We named these three fungal genetic clusters the blue Eastern, yellow Western and orange Western *Microbotryum* clusters, in reference to their *S. nutans* host plastid haplotypes. In contrast to the host plant *S. nutans*, we found no clear subdivision in the orange Western anther-smut fungal cluster (Fig S3). We found no genetic clusters specific to strains sampled from a host with a red haplotype, perhaps due to the low strain number. We excluded for further analyses the two admixed fungal strains (cluster memberships <0.80 in a given cluster) and the three fungal strains sampled on a host with a red haplotype. We found no further population structure in the set of 28 anther-smut strains parasitizing *S. italica* (Fig S4), as for the host plant.

All three fungal genetic clusters parasitizing *S. nutans* had similar levels of allelic richness (KWRS test on 16 groups of sites, $Chi^2 = 1.33$, df = 2, p-value = 0.514; Table S8B) and observed heterozygosity (KWRS test, $Chi^2 = 0.67$, df = 2, p-value = 0.716; Table S8B). The F_{IS} varied between genetic clusters from -0.11 to 0.82 (Table S8B). We found no significant differences in differentiation between the three fungal genetic clusters (KWRS tests for F_{ST} and Jost's D, $Chi^2 = 2$, df = 2, p-value = 0.368; Table S9B). The significant correlation between the matrices of genetic and geographic distances between pairs of fungal populations parasitizing *S. nutans* (16 sites) indicated an IBD pattern (Mantel test: r = 0.62, p-value < 0.001). There was a significantly positive correlation between genetic distance matrices for the fungal and the *S. nutans* populations (16 sites; Mantel test: r = 0.80, p-value < 0.001), and it remained significant when controlling for the IBD effect (partial Mantel test: r = 0.70, p-value < 0.001). Altogether, our findings indicate strong congruence between the population genetic structures of the anther-smut

fungi parasitizing *S. nutans* and its host plant *S. nutans* (Fig 3C). We found no signatures of recent reduction in effective population size in either of the three fungal genetic clusters parasitizing *S. nutans* nor the fungal genetic cluster parasitizing *S. italica* using the BOTTLENECK software (Piry et al., 1999) under either stepwise or two-phase models of microsatellite evolution (Table S10; one-tailed Wilcoxon signed rank test, all P-values>0.36).

Inferred divergence history of anther-smut fungi on *Silene nutans* congruent with of their host plant

To study if the anther-smut fungi on *S. nutans* shared the same history of divergence into cryptic lineages as the one previously inferred for their host plants, the *S. nutans* cryptic species complex (Martin et al., 2016; Martin et al., 2017; Van Rossum et al., 2018), we used an approximate Bayesian computation random forest (ABC-RF) procedure. We compared various divergence scenarios for the three identified *Microbotryum* genetic clusters parasitizing *S. nutans*. We removed the 21 fungal strains that were likely siblings of other fungal strains, keeping 110 anther-smut fungal strains belonging to the blue Eastern, yellow Western and orange Western *Microbotryum* genetic clusters parasitizing *S. nutans* and we used as outgroup the 25 genotyped *Microbotryum* strains parasitizing *S. italica.*

We performed three rounds of scenario comparison, each testing a particular evolutionary event, including divergence times, divergence order and the occurrence of gene flow (Table 1; Table S5; Fig S5). At each round, we retained the inferred most likely evolutionary scenario to be used as backbone for the subsequent rounds. To assess our power to discriminate between scenarios, we checked posterior probability (Table 1) and assessed visually whether the observed data fell

533 within the clouds of simulated data of the compared scenarios (Fig S6).

534 In the first round ("time of divergence"; Table 1, “round 1”), we tested four different time periods
535 of divergence for various divergence orders (A, B or C; Fig S5A). The group of scenarios with
536 strongest support included a first divergence occurring between 100,000-1,500,000 years ago,
537 and a second divergence occurring between 0-20,000 years ago (posterior probability = 0.54 +-
538 0.02, prior error rate = 34%; Table 1, “round 1”; Fig S6A). In the second round ("divergence
539 order"; Table 1, “round 2”), we found with a high posterior probability for the scenario assuming
540 a first divergence of the blue Eastern *Microbotryum* genetic cluster, followed by the divergence
541 between the yellow and orange Western *Microbotryum* genetic clusters (posterior probability =
542 0.79 +-0.02, prior error rate = 2%; Table 1, “round 2”; Fig S6B). When testing the order of
543 divergence between clusters as first round and the time of divergence as second round, we
544 selected the same scenarios with a high posterior probability (Note S1; Table S11).

545 In the third round ("occurrence of gene flow"; Table 1, “round 3, step 1”), we compared in a first
546 step three groups of scenarios differing in the clusters affected by gene flow. The most supported
547 group of scenarios assumed gene flow among *Microbotryum* genetic clusters parasitizing *S.*
548 *nutans* but not with *S. italica* (posterior probability = 0.60 +-0.02, prior error rate = 5%; Table 1,
549 “round 3, step 1”; Fig S6C). In the following steps (Table 1, “round 3, steps 2 to 4”), we
550 compared groups of scenarios of divergence with different timing of gene flow. Scenarios of
551 divergence with ancient gene flow were the most supported, which suggested that episodes of
552 ancient gene flow occurred during divergence or just following divergence of the three
553 *Microbotryum* genetic clusters parasitizing *S. nutans* and then completely stopped (posterior
554 probability = 0.76 +-0.02, prior error rate = 35%; Table 1, “round 3, step 2”; Fig S6D-F).
555 However, we did not have enough power to differentiate between scenarios of ancient gene flow

that involved different genetic clusters (either all three genetic clusters or only the two Western genetic clusters) or different times of past gene flow (either over a 0-20000 year period or a 50,000-500,000 year period; Table S5; posterior probability = 0.49 +-0.03, prior error rate = 60%; Table 1, "round 3, step 5"). We performed parameter inferences for the group of four models with ancient migration ("round 3, step 2", group 3 see Table 1; Table S12). The inferred dates and order of divergence between fungal genetic clusters parasitizing *S. nutans* were consistent with the history of divergence previously inferred for the host plant *S. nutans* (Fig 4; Martin et al., 2016; Martin et al., 2017; Van Rossum et al., 2018).

No genome-wide signatures of gene flow between anther-smut fungi on distinct *Silene* species

To check whether genome-wide data support the patterns inferred above on population genetic structure in the anther-smut fungi and lack of recent gene flow, we sequenced the genomes of 53 *Microbotryum* strains parasitizing *S. nutans* or *S. italica* (Table S7). We also used previously sequenced genomes of anther-smut fungi parasitizing species with overlapping geographical ranges in order to check if some of the strains that appeared as admixed or did not cluster according to their host species may actually correspond to other *Microbotryum* species. After filtration, we obtained 1,305,369 SNPs for 108 *Microbotryum* strains. We performed PCA analyses on the genome-wide SNPs and STRUCTURE analyses and confirmed strong population differentiation between fungal strains parasitizing *S. nutans* and *S. italica* (Fig 5A-B; Fig S7A). Only one strain parasitizing *S. nutans* clustered with strains parasitizing *S. italica,* similarly as found from microsatellite data (strain # 1438; Fig 2C), therefore likely being a genuine spill-over

578 between *S. nutans* and *S. italica*. Two other strains parasitizing *S. nutans* clustered with strains
579 parasitizing *S. latifolia.* These strains had admixed cluster membership (i.e. mean membership
580 coefficient <0.80 to the given cluster) or clustered with strains parasitizing *S. italica* from
581 microsatellite data (Fig 2C). These strains likely represent spill-overs between *S. nutans* and *S.*
582 *latifolia*.

583 Genome sequences retrieved the same genetic structure as microsatellites for anther-smut fungi
584 parasitizing *S. nutans,* with a strong differentiation between *Microbotryum* strains sampled on the
585 *S. nutans* blue plastid haplotype on the one hand and those sampled on yellow, red or orange
586 plastid haplotypes on the other hand (Fig S7B), and confirmed the absence of strong population
587 structure within anther-smut fungi parasitizing *S. italica* (Fig S7C). We also found strong
588 population differentiation between fungal strains parasitizing the three closely related host
589 species of *S. nutans* and *S. italica* (Fig 5A-B). STRUCTURE analyses showed no signatures of
590 recent admixture between strains parasitizing different hosts (Fig 5B).

591 The phylogenetic network analysis implemented in SplitsTree also supported the absence of
592 recent gene flow at the genome-wide levels between the *Microbotryum* species parasitizing
593 different hosts and the close genetic similarity of the three genetic clusters of anther-smut fungi
594 parasitizing the *S. nutans* complex (Fig 5C). Within *Microbotryum* strains parasitizing *S. nutans*,
595 we found no footprint of recombination between strains of the two main genetic clusters (Fig 5C)
596 which was consistent with a scenario of divergence with ancient migration and no contemporary
597 gene flow inferred from ABC demographic inferences.

598

599 **Discussion**

We found that genetic structure and divergence history of anther-smut fungi parasitizing the *S. nutans* plant species complex closely mirrored those of their host plant genetic lineages. Such a congruence in population structure and divergence history of the host and the pathogen in the *S. nutans* complex, the distribution area of the genetic clusters in Western Europe, as well as the inferred dates of divergence suggest that the host and the pathogen differentiated in parallel following isolation in shared glacial refugia. To confirm the co-divergence events between *S. nutans* lineages and anther-smut fungi genetic clusters, we need to more accurately date the node of lineage divergence events in the host and the pathogen. Such molecular dating is essential to support co-divergence events as preferential shifts of the pathogen to closely related host species can also produce congruent phylogenies (de Vienne et al., 2013), but is currently difficult due lack of appropriate calibration points.

Nevertheless, our results rule out the hypothesis that anther-smut fungi on some of the *S. nutans* genetic lineages may result from specialization by host shifts from distant anther-smut fungi parasitizing other *Silene* species in sympatry or parapatry. This contrasts with the prevalence of host shifts between distant lineages observed in the Caryophyllaceae-*Microbotryum* system at larger evolutionary scales (Refrégier et al., 2008), but is consistent with the strong congruence reported between the population genetic structures of *S. latifolia* and its anther-smut fungi, also corresponding to glacial refugia footprints (Feurtey et al., 2016). Our study thus contributes towards gaining general insights into the processes of divergence in host-pathogen systems. While at large evolutionary scales, host shifts seem to be the rule (de Vienne, Hood, & Giraud, 2009; Thines, 2019), finer and more recent population subdivisions may more often result from codivergence due to shared geographic and climatic constraints, such as glacial refugia. The discrepancy between the two evolutionary scales may be due to recurrent pathogen lineage

623 extinctions followed by recolonizations through host shifts: codivergence may occur frequently,
624 but pathogen lineages would regularly go extinct over longer evolutionary scales and plant
625 lineages would be recolonized by host shifts. This novel hypothesis can be tested by studying
626 further closely related pairs of natural host-pathogen associations, which unfortunately still
627 remain scarce.

628 The significant IBD pattern in both the *S. nutans* plant and anther-smut fungi and the correlation
629 between the genetic distances between host and pathogen pairs when controlling for IBD suggest
630 that the anther-smut fungi followed similar recolonization routes as the plant and/or became
631 specialized on the host genetic lineages. However, contrary to the system *S. latifolia* - *M.*
632 *lychnidis-dioicae* (Feurtey et al., 2016) and other host-pathogen systems (Barrett et al., 2008;
633 Criscione, Poulin, & Blouin, 2005; Nieberding et al., 2008; Nieberding & Olivieri, 2007), we
634 found higher levels of subdivision in *S. nutans* than in its associated anther-smut fungi. The
635 weaker genetic structure in anther smut fungi compared to its host suggests again extinction of
636 the pathogen lineage in a plant lineage, followed by recolonization from another fungal lineage,
637 or the ability of an anther-smut lineage to remain generalist on two closely related plant lineages.

638 Future studies using cross-inoculation experiments between strains and host plants of different
639 genetic clusters within the *S. nutans* complex could assess whether the congruence of host-
640 pathogen genetic structure is associated with a pattern of local adaptation of the pathogen or of
641 the host, as in the system *S. latifolia* - *M. lychnidis-dioicae* (Delmotte et al., 1999; Feurtey et al.,
642 2016; Kaltz et al., 1999). We could not obtain enough fresh material for this study to be able to
643 test local adaptation. Furthermore, strong asymmetric postzygotic reproductive isolation was
644 found between the Eastern and Western *S. nutans* plant lineages (Martin et al., 2017) and it would
645 be interesting in future studies to explore if a similar reproductive isolation pattern is present

between the Eastern and Western fungal lineages on *S. nutans*, and whether reproductive isolation can be found among anther-smut fungi.

We found clear differentiation between fungal populations parasitizing the two closely related *S. nutans* and *S. italica* species, supporting previous findings of differentiation based on a few strains and loci (Bucheli et al., 2000). No strong population structure was found within *S. italica* or within its associated anther-smut fungi. However, future studies with larger sampling distribution in the *S. italica* range in the Mediterranean Basin (Naciri, Pasquier, Lundberg, Jeanmonod, & Oxelman, 2017) may identify population differentiation. Cross-species disease transmissions, i.e. spill-overs of fungal strains, were more frequent on *S. nutans* than on *S. italica*, which may be due to unequal sampling size between the two *Silene* species or to biological differences. Some Caryophyllaceae plants indeed seem more susceptible to cross-species transmissions (Antonovics et al., 2002; de Vienne, Hood, et al., 2009; Hood et al., 2019). Putative spill-overs may actually correspond to other *Microbotryum* species, that were too rare to be identified in our population analyses using microsatellite markers, as revealed with the whole genome sequence data. In fact, two strains collected on *S. nutans* were actually assigned, based on whole genome sequences, to *M. lychnidis-dioicae,* specialized on *S. latifolia.*

The statistical comparison of demographic models and the whole-genome SNP analyses indicated the absence of recent gene flow between *Microbotryum* species parasitizing closely related *Silene* species, as well as between the Eastern and Western fungal lineages parasitizing *S. nutans*, although some spill-over cases were detected. Noteworthy, we also found no evidence of hybrid individuals between the two host plants species *S. nutans* and *S. italica* based on SNP data. The admixed barplots observed in the microsatellite STRUCTURE analyses must therefore have been due to low power of assignment rather than recent hybridization. This result was consistent with

669 previous studies on several other anther-smut fungi, in which no hybrids were detected in natural
670 populations, even between very closely related species that can hybridize in the laboratory
671 (Abbate et al., 2018; Badouin et al., 2017; Gladieux et al., 2013; Petit et al., 2017). The only case
672 where hybrids were detected was among closely related anther-smut fungi with overlapping host
673 and geographic ranges, on *Dianthus* species (Petit et al., 2017). Ecological factors, such as
674 different habitats, pollinator guilds or flowering time of the host species (Jürgens, Witt, &
675 Gottsberger, 1996; Kephart, Reynolds, Rutter, Fenster, & Dudash, 2006), may constitute pre-
676 zygotic factors favoring reproductive isolation of host-specialized anther-smut fungi in natural
677 populations. Both extrinsinc and intrinsic post-zygotic barriers can be strong in anther-smut fungi
678 (Giraud & Gourbière, 2012; Le Gac, Hood, & Giraud, 2007). Strong host specialization may
679 indeed play a role in reproductive isolation, through migrant inviability and hybrid maladaptation
680 on parental hosts, especially given the life cycle of *Microbotryum* fungi, with many spores falling
681 on a plant and competing for systemic infection, and selfing being frequent, exposing hybrids to
682 systematic competition with non-hybrids (Gibson, Hood, & Giraud, 2012). In addition,
683 comparative genomics of anther-smut fungi showed presence of large genomic rearrangements
684 and gene content variation between species (Branco et al., 2018; Hartmann et al., 2018), and
685 experimental crosses suggested high frequency of hybrid sterility and abnormal genomic contents
686 in hybrids (de Vienne, Refrégier, et al., 2009).

687 The low levels of gene flow among anther-smut fungi parasitizing different hosts found in
688 *Microbotryum* fungi stand in high contrast with frequent reports of signatures of introgression in
689 other fungal pathogens, such as crop pathogens or human disease-associated pathogens (Feurtey
690 & Stukenbrock, 2018). Few studies have focused on fungal pathogens diversification in natural
691 host communities while several evolutionary processes, such as time scale of divergence, host

692 density and heterogeneity, are likely very different than those occurring on human-modified
693 environment pathogens (Laine, 2005; Laine, Barrès, Numminen, & Siren, 2019; Stukenbrock &
694 McDonald, 2008). To understand how biodiversity arises and what the mechanisms of host-
695 pathogen evolution are over large evolutionary scales, we need more studies on co-evolutionary
696 histories of parasites and their hosts in natural ecosystems. Studies of population genetic structure
697 and divergence in plant fungal pathogens indeed remain so far mostly focused on crop pathogens
698 (Barrès et al., 2008; Enjalbert, Duan, Leconte, HovmøLler, & De Vallavieille-Pope, 2005;
699 Fournier & Giraud, 2008; Linde, Zhan, & McDonald, 2002; Saleh, Milazzo, Adreit, Fournier, &
700 Tharreau, 2014; Stukenbrock, Banke, & McDonald, 2006; Zaffarano, McDonald, & Linde,
701 2008), in which patterns are heavily impacted by host genetic homogeneity and high abundance,
702 as well as by human-mediated plant and pathogen dispersal. We found here strong population
703 structure congruence between hosts and pathogens, in agreement with a previous study on other
704 anther-smut lineages (Feurtey et al., 2016). Further studies on other natural systems are needed to
705 assess whether this represents a general pattern in natural pathogen-host communities.

706

707 **Acknowledgements**

708 We thank all the collectors cited in Table S1 and S7 for their contribution to plant material
709 sampling, the Département de la Nature et des Forêts (Service Public de Wallonie, Belgium), B.
710 Clesse (Centre Marie-Victorin, Cercles des Naturalistes de Belgique asbl), Ardenne & Gaume
711 and Natagora for access to natural sites and for the authorization to collect plant material. We are
712 grateful to the INRA MIGALE bioinformatics platform (http://migale.jouy.inra.fr) for providing
713 computational resources and the Genotoul platform for sequencing. We thank the Plateforme de
714 Genotypage GENTYANE INRA UMR1095 for help with microsatellite genotyping. This work

715 was supported by the European Research Council (ERC) (starting grant GenomeFun 309403), the
716 French National Research Agency (ANR) (Gandalf ANR Grant ANR-12-ADAP-0009), the Louis
717 D. Foundation (Institut de France) to TG, and a Marie Curie European grant (PRESTIGE-2016-4-
718 0013) to FEH. PT and CG thank the Région Hauts-de-France, and the Ministère de
719 l'Enseignement Supérieur et de la Recherche (CPER Climibio), and the European Fund for
720 Regional Economic Development for their financial support.

721

722 **Datasets**

723 dataset 1: Hartmann F.E., Snirc A., Cornille A., Godé C., Touzet P., Van Rossum F., Fournier E.,
724 Le Prieur S., Shykoff J., Giraud T. 2020. Genotype data from : Congruent population genetic
725 structures and divergence histories in anther-smut fungi and their host plants Silene italica and
726 the S. nutans species complex, Dryad, Dataset, https://doi.org/10.5061/dryad.m63xsj3z3

727 dataset 2: Hartmann F.E., Snirc A., Cornille A., Godé C., Touzet P., Van Rossum F., Fournier E.,
728 Le Prieur S., Shykoff J., Giraud T. 2020. Whole genome sequencing raw data of *Microbotryum*
729 fungi infecting *Silene nutans* and *S. italica*. NCBI Sequence Read Archive (SRA). BioProject ID
730 PRJNA589725.

731

732 **References**

733 Abbate, J. L., Gladieux, P., Hood, M. E., de Vienne, D. M., Antonovics, J., Snirc, A., & Giraud,
734 T. (2018). Co-occurrence among three divergent plant-castrating fungi in the same *Silene*
735 host species. *Molecular Ecology*, *27*(16), 3357–3370. doi: 10.1111/mec.14805
736 Antonovics, J., Hood, M. E., & Partain, J. (2002). The ecology and genetics of a host shift:
737 *Microbotryum* as a model system. *The American Naturalist*, *160*(S4), S40–S53. doi:
738 10.1086/342143
739 Badouin, H., Gladieux, P., Gouzy, J., Siguenza, S., Aguileta, G., Snirc, A., … Giraud, T. (2017).
740 Widespread selective sweeps throughout the genome of model plant pathogenic fungi and
741 identification of effector candidates. *Molecular Ecology*, *26*(7), 2041–2062. doi:
742 10.1111/mec.13976
743 Barrès, B., Halkett, F., Dutech, C., Andrieux, A., Pinon, J., & Frey, P. (2008). Genetic structure
744 of the poplar rust fungus *Melampsora larici-populina*: Evidence for isolation by distance
745 in Europe and recent founder effects overseas. *Infection, Genetics and Evolution*, *8*(5),

577–587. doi: 10.1016/j.meegid.2008.04.005
Barrett, L. G., Thrall, P. H., Burdon, J. J., & Linde, C. C. (2008). Life history determines genetic structure and evolutionary potential of host–parasite interactions. *Trends in Ecology & Evolution*, *23*(12), 678–685. doi: 10.1016/j.tree.2008.06.017
Becker, R., Wilks, A., Brownrigg, R., Minka, T., & Deckmyn, D. (2017). *maps: draw geographical maps. R package version 3.2.0.* (https://cran.r-project.org/web/packages/maps/index.html).
Bernasconi, G., Antonovics, J., Biere, A., Charlesworth, D., Delph, L. F., Filatov, D., … Widmer, A. (2009). *Silene* as a model system in ecology and evolution. *Heredity*, *103*(1), 5–14. doi: 10.1038/hdy.2009.34
Branco, S., Badouin, H., Rodríguez de la Vega, R. C., Gouzy, J., Carpentier, F., Aguileta, G., … Giraud, T. (2017). Evolutionary strata on young mating-type chromosomes despite the lack of sexual antagonism. *Proceedings of the National Academy of Sciences*, *114*(27), 7067–7072. doi: 10.1073/pnas.1701658114
Branco, S., Carpentier, F., Rodríguez de la Vega, R. C., Badouin, H., Snirc, A., Prieur, S. L., … Giraud, T. (2018). Multiple convergent supergene evolution events in mating-type chromosomes. *Nature Communications*, *9*(1), 2000. doi: 10.1038/s41467-018-04380-9
Breiman, L. (2001). Random forests. *Machine Learning*, *45*(1), 5–32. doi: 10.1023/A:1010933404324
Bucheli, E., Gautschi, B., & Shykoff, J. A. (2000). Host-specific differentiation in the anther smut fungus *Microbotryum violaceum* as revealed by microsatellites. *J. EVOL. BIOL.*, 11.
Chang, C. C., Chow, C. C., Tellier, L. C., Vattikuti, S., Purcell, S. M., & Lee, J. J. (2015). Second-generation PLINK: rising to the challenge of larger and richer datasets. *GigaScience*, *4*(1). doi: 10.1186/s13742-015-0047-8
Cornille, A., Gladieux, P., Smulders, M. J. M., Roldán-Ruiz, I., Laurens, F., Le Cam, B., … Giraud, T. (2012). New insight into the history of domesticated apple: Secondary contribution of the European wild apple to the genome of cultivated varieties. *PLOS Genetics*, *8*(5), e1002703. doi: 10.1371/journal.pgen.1002703
Criscione, C. D., Poulin, R., & Blouin, M. S. (2005). Molecular ecology of parasites: elucidating ecological and microevolutionary processes. *Molecular Ecology*, *14*(8), 2247–2257. doi: 10.1111/j.1365-294X.2005.02587.x
Croll, D., & Laine, A.-L. (2016). What the population genetic structures of host and pathogen tell us about disease evolution. *New Phytologist*, *212*(3), 537–539. doi: 10.1111/nph.14203
de Vienne, D. M., Hood, M. E., & Giraud, T. (2009). Phylogenetic determinants of potential host shifts in fungal pathogens. *Journal of Evolutionary Biology*, *22*(12), 2532–2541. doi: 10.1111/j.1420-9101.2009.01878.x
de Vienne, D. M., Refrégier, G., Hood, M. E., Guigue, A., Devier, B., Vercken, E., … Giraud, T. (2009). Hybrid sterility and inviability in the parasitic fungal species complex *Microbotryum*. *Journal of Evolutionary Biology*, *22*(4), 683–698. doi: 10.1111/j.1420-9101.2009.01702.x
de Vienne, D. M., Refrégier, G., López-Villavicencio, M., Tellier, A., Hood, M. E., & Giraud, T. (2013). Cospeciation vs host-shift speciation: methods for testing, evidence from natural associations and relation to coevolution. *New Phytologist*, *198*(2), 347–385. doi: 10.1111/nph.12150
Delmotte, F., Bucheli, E., & Shykoff, J. A. (1999). Host and parasite population structure in a natural plant–pathogen system. *Heredity*, *82*(3), 300–308. doi: 10.1046/j.1365-2540.1999.00485.x

Dray, S., & Dufour, A.-B. (2007). The ade4 Package: Implementing the Duality Diagram for Ecologists. *Journal of Statistical Software*, *22*(1), 1–20. doi: 10.18637/jss.v022.i04

Dybdahl, M. F., & Lively, C. M. (1996). The geography of coevolution: comparative population structures for a snail and its trematode parasite. *Evolution*, *50*(6), 2264–2275. doi: 10.1111/j.1558-5646.1996.tb03615.x

Enjalbert, J., Duan, X., Leconte, M., HovmøLler, M. S., & De Vallavieille-Pope, C. (2005). Genetic evidence of local adaptation of wheat yellow rust (*Puccinia striiformis* f. sp. *tritici*) within France. *Molecular Ecology*, *14*(7), 2065–2073. doi: 10.1111/j.1365-294X.2005.02566.x

Estoup, A., Jarne, P., & Cornuet, J.-M. (2002). Homoplasy and mutation model at microsatellite loci and their consequences for population genetics analysis. *Molecular Ecology*, *11*(9), 1591–1604. doi: 10.1046/j.1365-294X.2002.01576.x

Estoup, A., Raynal, L., Verdu, P., & Marin, J.-M. (2018). Model choice using Approximate Bayesian Computation and Random Forests: analyses based on model grouping to make inferences about the genetic history of Pygmy human populations | Journal de la Société Française de Statistique. *Special Issue on Models and Inference in Population Genetics*, *159*(3). Retrieved from http://journal-sfds.fr/article/view/709

Excoffier, L., & Foll, M. (2011). fastsimcoal: a continuous-time coalescent simulator of genomic diversity under arbitrarily complex evolutionary scenarios. *Bioinformatics*, *27*(9), 1332–1334. doi: 10.1093/bioinformatics/btr124

Excoffier, L., & Lischer, H. E. L. (2010). Arlequin suite ver 3.5: a new series of programs to perform population genetics analyses under Linux and Windows. *Molecular Ecology Resources*, *10*(3), 564–567. doi: 10.1111/j.1755-0998.2010.02847.x

Feurtey, A., Gladieux, P., Hood, M. E., Snirc, A., Cornille, A., Rosenthal, L., & Giraud, T. (2016). Strong phylogeographic co-structure between the anther-smut fungus and its white campion host. *New Phytologist*, *212*(3), 668–679. doi: 10.1111/nph.14125

Feurtey, A., & Stukenbrock, E. H. (2018). Interspecific gene exchange as a driver of adaptive evolution in fungi. *Annual Review of Microbiology*, *72*(1), 377–398. doi: 10.1146/annurev-micro-090817-062753

Fisher, M. C., Gow, N. A. R., & Gurr, S. J. (2016). Tackling emerging fungal threats to animal health, food security and ecosystem resilience. *Phil. Trans. R. Soc. B*, *371*(1709), 20160332. doi: 10.1098/rstb.2016.0332

Fortuna, T. M., Snirc, A., Badouin, H., Gouzy, J., Siguenza, S., Esquerre, D., … Giraud, T. (2016). Polymorphic microsatellite markers for the tetrapolar anther-smut fungus *Microbotryum saponariae* based on genome sequencing. *PLOS ONE*, *11*(11), e0165656. doi: 10.1371/journal.pone.0165656

Fournier, E., & Giraud, T. (2008). Sympatric genetic differentiation of a generalist pathogenic fungus, Botrytis cinerea, on two different host plants, grapevine and bramble. *Journal of Evolutionary Biology*, *21*(1), 122–132. doi: 10.1111/j.1420-9101.2007.01462.x

Gandon, S., & Michalakis, Y. (2002). Local adaptation, evolutionary potential and host–parasite coevolution: interactions between migration, mutation, population size and generation time. *Journal of Evolutionary Biology*, *15*(3), 451–462. doi: 10.1046/j.1420-9101.2002.00402.x

Gandon, S., Capowiez, Y., Dubois, Y., Michalakis, Y., & Olivieri, I. (1996). Local adaptation and gene-for-gene coevolution in a metapopulation model. *Proceedings of the Royal Society of London. Series B: Biological Sciences*, *263*(1373), 1003–1009. doi: 10.1098/rspb.1996.0148

Gerritsen, H. (2013). *Mapplots, r package version 1.5*. https://CRAN.R-project.org/package=mapplots.

Gibson, A. K., Hood, M. E., & Giraud, T. (2012). Sibling competition arena: selfing and a competition arena can combine to constitute a barrier to gene flow in sympatry. *Evolution*, *66*(6), 1917–1930. doi: 10.1111/j.1558-5646.2011.01563.x

Giraud, T. (2004). Patterns of within population dispersal and mating of the fungus *Microbotryum violaceum* parasitising the plant *Silene latifolia*. *Heredity*, *93*(6), 559–565. doi: 10.1038/sj.hdy.6800554

Giraud, T., & Gourbière, S. (2012). The tempo and modes of evolution of reproductive isolation in fungi. *Heredity*, *109*(4), 204–214. doi: 10.1038/hdy.2012.30

Giraud, T., Yockteng, R., Marthey, S., Chiapello, H., Jonot, O., Lopez-Villavicencio, M., … Dossat, C. (2008). Isolation of 60 polymorphic microsatellite loci in EST libraries of four sibling species of the phytopathogenic fungal complex *Microbotryum*. *Molecular Ecology Resources*, *8*(2), 387–392. doi: 10.1111/j.1471-8286.2007.01967.x

Gladieux, P., Devier, B., Aguileta, G., Cruaud, C., & Giraud, T. (2013). Purifying selection after episodes of recurrent adaptive diversification in fungal pathogens. *Infection, Genetics and Evolution: Journal of Molecular Epidemiology and Evolutionary Genetics in Infectious Diseases*, *17*, 123–131. doi: 10.1016/j.meegid.2013.03.012

Gladieux, P., Vercken, E., Fontaine, M. C., Hood, M. E., Jonot, O., Couloux, A., & Giraud, T. (2011). Maintenance of fungal pathogen species that are specialized to different hosts: allopatric divergence and introgression through secondary contact. *Molecular Biology and Evolution*, *28*(1), 459–471. doi: 10.1093/molbev/msq235

Godé, C., Touzet, P., Martin, H., Lahiani, E., Delph, L. F., & Arnaud, J.-F. (2014). Characterization of 24 polymorphic microsatellite markers for *Silene nutans*, a gynodioecious–gynomonoecious species, and cross-species amplification in other *Silene* species. *Conservation Genetics Resources*, *6*(4), 915–918. doi: 10.1007/s12686-014-0240-6

Hafner, M. S., Page, R. D. M. (1995). Molecular phylogenies and host-parasite cospeciation: gophers and lice as a model system. *Philosophical Transactions of the Royal Society of London. Series B: Biological Sciences*, *349*(1327), 77–83. doi: 10.1098/rstb.1995.0093

Hartmann, F. E., Rodríguez de la Vega, R. C., Brandenburg, J.-T., Carpentier, F., & Giraud, T. (2018). Gene presence–absence polymorphism in castrating anther-smut fungi: recent gene gains and phylogeographic structure. *Genome Biology and Evolution*, *10*(5), 1298–1314. doi: 10.1093/gbe/evy089

Hartmann, F. E., Rodríguez de la Vega, R. C., Carpentier, F., Gladieux, P., Cornille, A., Hood, M. E., & Giraud, T. (2019). Understanding adaptation, coevolution, host specialization, and mating system in castrating anther-smut fungi by combining population and comparative genomics. *Annual Review of Phytopathology*, *57*(1), 431–457. doi: 10.1146/annurev-phyto-082718-095947

Hood, M. E., Antonovics, J., Wolf, M., Stern, Z. L., Giraud, T., & Abbate, J. L. (2019). Sympatry and interference of divergent *Microbotryum* pathogen species. *Ecology and Evolution*, *0*(0). doi: 10.1002/ece3.5140

Huson, D. H. (1998). SplitsTree: analyzing and visualizing evolutionary data. *Bioinformatics (Oxford, England)*, *14*(1), 68–73.

Huson, D. H., & Bryant, D. (2006). Application of phylogenetic networks in evolutionary studies. *Molecular Biology and Evolution*, *23*(2), 254–267. doi: 10.1093/molbev/msj030

Jakobsson, M., & Rosenberg, N. A. (2007). CLUMPP: a cluster matching and permutation

887 program for dealing with label switching and multimodality in analysis of population
888 structure. *Bioinformatics*, *23*(14), 1801–1806. doi: 10.1093/bioinformatics/btm233
889 Jombart, T. (2008). adegenet: a R package for the multivariate analysis of genetic markers.
890 *Bioinformatics*, *24*(11), 1403–1405. doi: 10.1093/bioinformatics/btn129
891 Jombart, T., & Ahmed, I. (2011). adegenet 1.3-1: new tools for the analysis of genome-wide SNP
892 data. *Bioinformatics*, *27*(21), 3070–3071. doi: 10.1093/bioinformatics/btr521
893 Jürgens, A., Witt, T., & Gottsberger, G. (1996). Reproduction and pollination in central European
894 populations of *Silene* and *Saponaria* species. *Botanica Acta*, *109*(4), 316–324. doi:
895 10.1111/j.1438-8677.1996.tb00579.x
896 Kaltz, O., Gandon, S., Michalakis, Y., & Shykoff, J. A. (1999). Local maladaptation in the
897 anther-smut fungus *Microbotryum violaceum* to its host plant *Silene latifolia*: evidence
898 from a cross-inoculation experiment. *Evolution; International Journal of Organic*
899 *Evolution*, *53*(2), 395–407. doi: 10.1111/j.1558-5646.1999.tb03775.x
900 Keenan, K., McGinnity, P., Cross, T. F., Crozier, W. W., & Prodöhl, P. A. (2016). diveRsity: An
901 R package for the estimation and exploration of population genetics parameters and their
902 associated errors. *Methods in Ecology and Evolution*, 782–788. doi: 10.1111/2041-
903 210X.12067@10.1111/(ISSN)2041-210X.ecologyandevolutionireland
904 Kemler, M., Göker, M., Oberwinkler, F., & Begerow, D. (2006). Implications of molecular
905 characters for the phylogeny of the Microbotryaceae (Basidiomycota: Urediniomycetes).
906 *BMC Evolutionary Biology*, *6*, 35. doi: 10.1186/1471-2148-6-35
907 Kephart, S., Reynolds, R. J., Rutter, M. T., Fenster, C. B., & Dudash, M. R. (2006). Pollination
908 and seed predation by moths on *Silene* and allied Caryophyllaceae: evaluating a model
909 system to study the evolution of mutualisms. *New Phytologist*, *169*(4), 667–680. doi:
910 10.1111/j.1469-8137.2005.01619.x
911 Lafuma, L., & Maurice, S. (2006). Reproductive characters in a gynodioecious species, *Silene*
912 *italica* (Caryophyllaceae), with attention to the gynomonoecious phenotype. *Biological*
913 *Journal of the Linnean Society*, *87*(4), 583–591. doi: 10.1111/j.1095-8312.2006.00597.x
914 Lahiani, E., Dufaÿ, M., Castric, V., Le Cadre, S., Charlesworth, D., Van Rossum, F., & Touzet,
915 P. (2013). Disentangling the effects of mating systems and mutation rates on cytoplamic
916 diversity in gynodioecious *Silene nutans* and dioecious *Silene otites*. *Heredity*, *111*(2),
917 157–164. doi: 10.1038/hdy.2013.32
918 Laine, A.-L. (2005). Spatial scale of local adaptation in a plant-pathogen metapopulation. *Journal*
919 *of Evolutionary Biology*, *18*(4), 930–938. doi: 10.1111/j.1420-9101.2005.00933.x
920 Laine, A.-L. (2008). Temperature-mediated patterns of local adaptation in a natural plant–
921 pathogen metapopulation. *Ecology Letters*, *11*(4), 327–337. doi: 10.1111/j.1461-
922 0248.2007.01146.x
923 Laine, A.-L., Barrès, B., Numminen, E., & Siren, J. P. (2019). Variable opportunities for
924 outcrossing result in hotspots of novel genetic variation in a pathogen metapopulation.
925 *ELife*, *8*. doi: 10.7554/eLife.47091
926 Langmead, B., Trapnell, C., Pop, M., & Salzberg, S. L. (2009). Ultrafast and memory-efficient
927 alignment of short DNA sequences to the human genome. *Genome Biology*, *10*(3), R25.
928 doi: 10.1186/gb-2009-10-3-r25
929 Le Gac, M., Hood, M. E., Fournier, E., & Giraud, T. (2007). Phylogenetic evidence of host-
930 specific cryptic species in the anther smut fungus. *Evolution; International Journal of*
931 *Organic Evolution*, *61*(1), 15–26. doi: 10.1111/j.1558-5646.2007.00002.x
932 Le Gac, M., Hood, M. E., & Giraud, T. (2007). Evolution of reproductive isolation within a
933 parasitic fungal species complex. *Evolution*, *61*(7), 1781–1787. doi: 10.1111/j.1558-

5646.2007.00144.x
Linde, C. C., Zhan, J., & McDonald, B. A. (2002). Population structure of *Mycosphaerella graminicola*: from lesions to continents. *Phytopathology*, *92*(9), 946–955. doi: 10.1094/PHYTO.2002.92.9.946
Liu, S., Cornille, A., Decroocq, S., Tricon, D., Chague, A., Eyquard, J.-P., … Decroocq, V. (2019). From hybrid speciation of wild Armeniaca species to multiple domestication events in Eastern Asia: the complex evolutionary history of apricots. *Under Review*.
López-Villavicencio, M., Jonot, O., Coantic, A., Hood, M. E., Enjalbert, J., & Giraud, T. (2007). Multiple infections by the anther smut pathogen are frequent and involve related strains. *PLOS Pathogens*, *3*(11), e176. doi: 10.1371/journal.ppat.0030176
Lutz, M., Göker, M., Piatek, M., Kemler, M., Begerow, D., & Oberwinkler, F. (2005). Anther smuts of Caryophyllaceae: Molecular characters indicate host-dependent species delimitation. *Mycological Progress*, *4*(3), 225–238. doi: 10.1007/s11557-006-0126-4
Martin, M. (2011). Cutadapt removes adapter sequences from high-throughput sequencing reads. *EMBnet.Journal*, *17*(1), 10–12. doi: 10.14806/ej.17.1.200
Martin, H., Touzet, P., Dufay, M., Godé, C., Schmitt, E., Lahiani, E., … Rossum, F. V. (2017). Lineages of *Silene nutans* developed rapid, strong, asymmetric postzygotic reproductive isolation in allopatry. *Evolution*, *71*(6), 1519–1531. doi: 10.1111/evo.13245
Martin, H., Touzet, P., Van Rossum, F., Delalande, D., & Arnaud, J.-F. (2016). Phylogeographic pattern of range expansion provides evidence for cryptic species lineages in *Silene nutans* in Western Europe. *Heredity*, *116*(3), 286–294. doi: 10.1038/hdy.2015.100
McCoy, K. D., Boulinier, T., & Tirard, C. (2005). Comparative host–parasite population structures: disentangling prospecting and dispersal in the black-legged kittiwake Rissa tridactyla. *Molecular Ecology*, *14*(9), 2825–2838. doi: 10.1111/j.1365-294X.2005.02631.x
McDonald, B. A., & Stukenbrock, E. H. (2016). Rapid emergence of pathogens in agro-ecosystems: global threats to agricultural sustainability and food security. *Phil. Trans. R. Soc. B*, *371*(1709), 20160026. doi: 10.1098/rstb.2016.0026
McKenna, A., Hanna, M., Banks, E., Sivachenko, A., Cibulskis, K., Kernytsky, A., … DePristo, M. A. (2010). The Genome Analysis Toolkit: a MapReduce framework for analyzing next-generation DNA sequencing data. *Genome Research*, *20*(9), 1297–1303. doi: 10.1101/gr.107524.110
Michalakis, Y., Sheppard, A. W., Noel, V., & Olivieri, I. (1993). Population structure of a herbivorous insect and its host plant on a microgeographic scale. *Evolution*, *47*(5), 1611–1616. doi: 10.2307/2410172
Naciri, Y., Pasquier, P.-E. D., Lundberg, M., Jeanmonod, D., & Oxelman, B. (2017). A phylogenetic circumscription of *Silene* sect. *Siphonomorpha* (Caryophyllaceae) in the Mediterranean Basin. *Taxon*, *66*(1), 91–108. doi: 10.12705/661.5
Nei, M. (1972). Genetic distance between populations. *The American Naturalist*, *106*(949), 283–292. doi: 10.1086/282771
Nieberding, C. M., Durette-Desset, M.-C., Vanderpoorten, A., Casanova, J. C., Ribas, A., Deffontaine, V., … Michaux, J. R. (2008). Geography and host biogeography matter for understanding the phylogeography of a parasite. *Molecular Phylogenetics and Evolution*, *47*(2), 538–554. doi: 10.1016/j.ympev.2008.01.028
Nieberding, C. M., & Olivieri, I. (2007). Parasites: proxies for host genealogy and ecology? *Trends in Ecology & Evolution*, *22*(3), 156–165. doi: 10.1016/j.tree.2006.11.012
Paradis, E., Claude, J., & Strimmer, K. (2004). APE: Analyses of Phylogenetics and Evolution in

R language. *Bioinformatics*, *20*(2), 289–290. doi: 10.1093/bioinformatics/btg412
Petit, E., Silver, C., Cornille, A., Gladieux, P., Rosenthal, L., Bruns, E., … Hood, M. E. (2017). Co-occurrence and hybridization of anther-smut pathogens specialized on *Dianthus* hosts. *Molecular Ecology*, *26*(7), 1877–1890. doi: 10.1111/mec.14073
Piry, S., Luikart, G., & Cornuet, J. M. (1999). *BOTTLENECK: A computer program for detecting recent reductions in the effective population size using allele frequency data*. *90*, 502–503.
Poulin, R. (2005). *Parasite biodiversity*. Smithsonian Institution.
Pritchard, J. K., Stephens, M., & Donnelly, P. (2000). Inference of population structure using multilocus genotype data. *Genetics*, *155*(2), 945–959.
Pudlo, P., Marin, J.-M., Estoup, A., Cornuet, J.-M., Gautier, M., & Robert, C. P. (2016). Reliable ABC model choice via random forests. *Bioinformatics*, *32*(6), 859–866. doi: 10.1093/bioinformatics/btv684
Purcell, S., Neale, B., Todd-Brown, K., Thomas, L., Ferreira, M. A. R., Bender, D., … Sham, P. C. (2007). PLINK: A tool set for whole-genome association and population-based linkage analyses. *The American Journal of Human Genetics*, *81*(3), 559–575. doi: 10.1086/519795
Rameau, J.-C., Mansion, D., & Dumé, G. (1989). *Flore forestière française: Plaines et collines*. Forêt privée française.
Rameau, J.-C., Mansion, D., & Dumé, G. (2008). *Flore forestière française: guide écologique illustré. Région méditerranéenne*. Forêt privée française.
Raynal, L., Marin, J.-M., Pudlo, P., Ribatet, M., Robert, C. P., & Estoup, A. (2019). ABC random forests for Bayesian parameter inference. *Bioinformatics*, *35*(10), 1720–1728. doi: 10.1093/bioinformatics/bty867
Refrégier, G., Le Gac, M., Jabbour, F., Widmer, A., Shykoff, J. A., Yockteng, R., … Giraud, T. (2008). Cophylogeny of the anther smut fungi and their caryophyllaceous hosts: prevalence of host shifts and importance of delimiting parasite species for inferring cospeciation. *BMC Evolutionary Biology*, *8*, 100. doi: 10.1186/1471-2148-8-100
Saleh, D., Milazzo, J., Adreit, H., Fournier, E., & Tharreau, D. (2014). South-East Asia is the center of origin, diversity and dispersion of the rice blast fungus, *Magnaporthe oryzae*. *New Phytologist*, *201*(4), 1440–1456. doi: 10.1111/nph.12627
Stukenbrock, E. H., Banke, S., & McDonald, B. A. (2006). Global migration patterns in the fungal wheat pathogen *Phaeosphaeria nodorum*. *Molecular Ecology*, *15*(10), 2895–2904. doi: 10.1111/j.1365-294X.2006.02986.x
Stukenbrock, E. H., & McDonald, B. A. (2008). The origins of plant pathogens in agro-ecosystems. *Annual Review of Phytopathology*, *46*(1), 75–100. doi: 10.1146/annurev.phyto.010708.154114
Szpiech, Z. A., Jakobsson, M., & Rosenberg, N. A. (2008). ADZE: a rarefaction approach for counting alleles private to combinations of populations. *Bioinformatics*, *24*(21), 2498–2504. doi: 10.1093/bioinformatics/btn478
Taylor, D. R., & Keller, S. R. (2007). Historical range expansion determines the phylogenetic diversity introduced during contemporary species invasion. *Evolution*, *61*(2), 334–345. doi: 10.1111/j.1558-5646.2007.00037.x
Tellier, A., de Vienne, D. M., Giraud, T., Hood, M. E., & Refrégier, G. (2010). Theory and examples of reciprocal influence between hosts and pathogens, from short-term to long term interactions: coevolution, cospeciation and pathogen speciation following host shifts. In *Immunology and Immune System Disorders*. *Host-Pathogen Interactions: Genetics,*

Immunology and Physiology (Nova Science Publishers, pp. 37–77). NY: Barton AW.
Thines, M. (2019). An evolutionary framework for host shifts – jumping ships for survival. *New Phytologist*, *224*(2), 605–617. doi: 10.1111/nph.16092
Thompson, J. N. (2005). *The geographic mosaic of coevolution*. University of Chicago Press.
Thrall, P., Biere, A., & Antonovics, J. (1993). Plant life-history and disease susceptibility - the occurrence of Ustilago-Violacea on different species within the Caryophyllaceae. *Journal of Ecology*, *81*(3), 489–498. doi: 10.2307/2261527
Tison, J., & de Foucault, B. (2014). *Flora gallica: flore de France* (Biotope).
Toh, S. S., & Perlin, M. H. (2016). Resurgence of less-studied smut fungi as models of phytopathogenesis in the omics age. *Phytopathology*, *106*(11), 1244–1254. doi: 10.1094/PHYTO-02-16-0075-RVW
Tsai, Y.-H. E., & Manos, P. S. (2010). Host density drives the postglacial migration of the tree parasite, Epifagus virginiana. *Proceedings of the National Academy of Sciences*, *107*(39), 17035–17040. doi: 10.1073/pnas.1006225107
Tutin, T., Heywood, V., Burges, N., Valentine, D., Walters, S., & Webb, D. (2001). *Flora Europaea*. Royaume-Uni: Cambridge University Press.
Van Rossum, F., Martin, H., Le Cadre, S., Brachi, B., Christenhusz, M. J. M., & Touzet, P. (2018). Phylogeography of a widely distributed species reveals a cryptic assemblage of distinct genetic lineages needing separate conservation strategies. *Perspectives in Plant Ecology, Evolution and Systematics*, *35*, 44–51. doi: 10.1016/j.ppees.2018.10.003
Vercken, E., Fontaine, M. C., Gladieux, P., Hood, M. E., Jonot, O., & Giraud, T. (2010). Glacial refugia in pathogens: European genetic structure of anther smut pathogens on *Silene latifolia* and *Silene dioica*. *PLOS Pathogens*, *6*(12), e1001229. doi: 10.1371/journal.ppat.1001229
Wegmann, D., Leuenberger, C., Neuenschwander, S., & Excoffier, L. (2010). ABCtoolbox: a versatile toolkit for approximate Bayesian computations. *BMC Bioinformatics*, *11*(1), 116. doi: 10.1186/1471-2105-11-116
Wickham, H. (2009). *ggplot2: elegant graphics for data analysis*. Springer Science & Business Media.
Wilson, D. J., Falush, D., & McVean, G. (2005). Germs, genomes and genealogies. *Trends in Ecology & Evolution*, *20*(1), 39–45. doi: 10.1016/j.tree.2004.10.009
Wolfe, N. D., Dunavan, C. P., & Diamond, J. (2007). Origins of major human infectious diseases. *Nature*, *447*(7142), 279–283. doi: 10.1038/nature05775
Zaffarano, P. L., McDonald, B. A., & Linde, C. C. (2008). Rapid speciation following recent host shifts in the plant pathogenic fungus *Rhynchosporium*. *Evolution*, *62*(6), 1418–1436. doi: 10.1111/j.1558-5646.2008.00390.x

Data accessibility

The plant microsatellite and chloroplastic genotypes and the fungal microsatellite genotypes are available at Dryad, Dataset, https://doi.org/10.5061/dryad.m63xsj3z3. We deposited the genome

raw data at NCBI Sequence Read Archive (SRA) under the BioProject ID PRJNA589725 (see Table S7 for BioSample accession numbers).

Author contributions

TG and FH conceived and designed the project with the help of FVR. TG, PT, FVR, JS and EF collected samples. AS, CG, PT, SLP and FH genotyped the samples. FH and AC performed the analyses. FH, TG and FVR wrote the manuscript. All authors read and approved the final version of the manuscript and declare no conflict of interest.

Supporting information

Additional Supporting Information may be found in the online version of this article.

Tables

Table 1: Comparisons of scenarios and group of scenarios used for approximate Bayesian computation (ABC) to reconstruct the fungi divergence history. Scenarios are described in Table S5 and Fig S5. Results of ABC random forest procedure are shown, with the percentage of vote for each scenario/group of scenarios, the posterior probability and the prior error rate. The best scenario is indicated with bold and three stars in the percentage of vote.

Figures

Figure 1: Population genetic structure of *Silene nutans* and *S. italica* host plants based on six plastid (chloroplast) SNPs and 21 microsatellite markers. A. Plastid haplotypes according to their geographic distribution. On the right, a zoom of the map in the northeastern region of France and Belgium is shown. The size of the symbols is proportional to the number of individuals sampled by site (1-9 plants). B. Principal component analysis (PCA), with information of plastid haplotypes. The first and second principal component axes are shown and the percentage of variance explained by each axis is indicated into brackets. C. Results of STRUCTURE on both host plant species for K=5 clusters. On panels A and B, symbol shape indicates species and color indicates plastid haplotypes. The two genetic clusters identified within the orange plastid haplotype based on the STRUCTURE analysis (panel C) are shown with light and dark orange colors, respectively.

Figure 2: Population genetic structure of anther-smut fungi (*Microbotryum*) parasitizing *Silene nutans* and *S. italica* based on 22 microsatellite markers. A. Anther-smut fungi parasitizing *S. italica* (top; photo credit M.E. Hood) and *S. nutans* (bottom; photo credit M. Strack van Schijndel). B. Principal component analysis (PCA). The first and second principal component axes are shown and the percentage of variance explained by each axis is indicated into brackets. The symbol shape indicates the sampling host species. The dark and light blue colors indicate assignment probability >0.80 to the two corresponding clusters identified in the STRUCTURE analysis for K=2 (see panel C). Pink color indicates strains for which no cluster could be assigned with a probability >0.80. Genetic variance explained by the principal component axes is shown in the right bottom corner. C. STRUCTURE barplot for K=2. Strains are ordered according to their sampling host species.

Figure 3: Congruence of population genetic structure between *Silene nutans* host plants and their anther-smut fungal (*Microbotryum*) strains based on microsatellite markers. A. Principal component analysis (PCA) on the fungal strains with information of the population genetic structure of their hosts. The first and second principal component axes are shown. Symbol shape indicates the sampling host species and color indicates the plastid haplotypes of the sampling host. B. STRUCTURE barplots for (1) K=3 in 112 *Microbotryum* strains and (2) K=4 in 110 *S. nutans* plant individuals. Fungal strains are ordered according to their sampling host plastid haplotypes. Host plant individuals are ordered according to their plastid haplotypes. C. Map of mean cluster membership proportions per site for (1) the 112 fungal strains in the STRUCTURE analysis at K=3 and (2) the 110 *S. nutans* plant individuals in the STRUCTURE analysis at K=4. The pie diameter reflects the sample size in the corresponding site (1 - 14 individuals).

Figure 4: Most likely scenario for the divergence between the fungal genetic clusters inferred with approximate Bayesian computation (ABC).

Figure 5: Absence of genome-wide signature of recent gene flow among anther-smut fungal strains parasitizing closely related *Silene* species. A. Principal component analysis (PCA) based on 1,305,369 genome-wide SNPs. B. STRUCTURE analyses based on 233 unlinked SNPs for K=5. The Y axis indicates the estimated membership proportions in the *K* clusters for each fungal strain (X axis). C. Neighbornet tree from a SplitsTree analysis based on 595,002 genome-wide SNPs with no missing data and heterozygote genotypes. The inner plot shows a zoom of the tip of the tree for strains parasitizing *S. nutans*. Information on the species or plastid haplotype of the host of sampling of the strains is given.

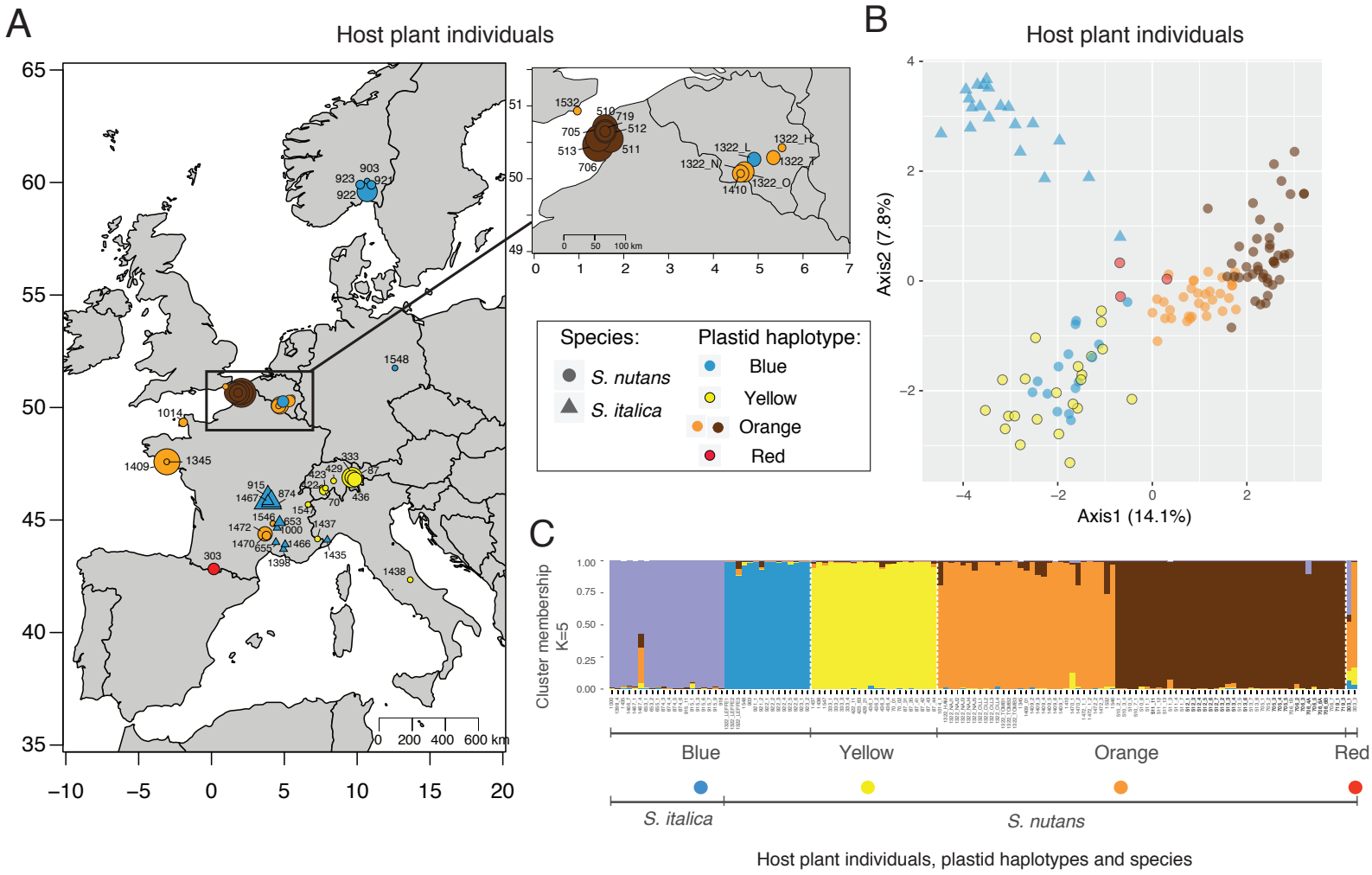
A
Host plant individuals
B
Host plant individuals
Species:
S. nutans
S. italica
Plastid haplotype:
Blue
Yellow
Orange
Red
Axis1 (14.1%)
Axis2 (7.8%)
C
Cluster membership
K=5
Blue
Yellow
Orange
Red
S. italica
S. nutans
Host plant individuals, plastid haplotypes and species

A

B

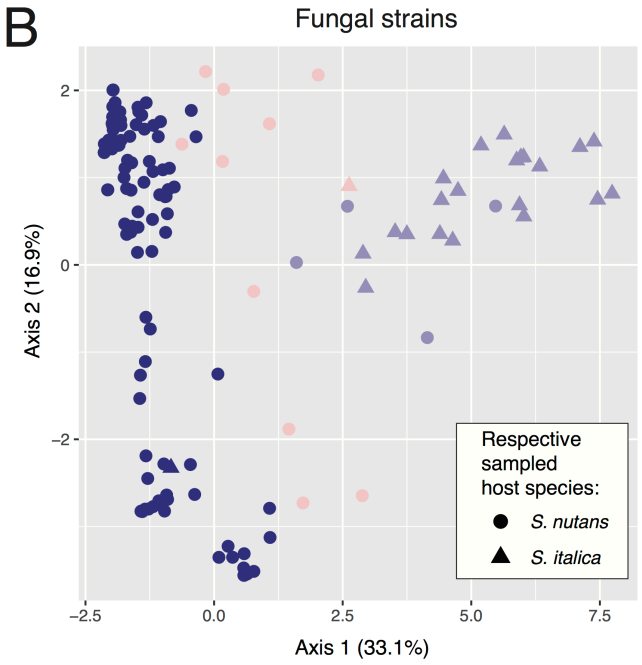

C

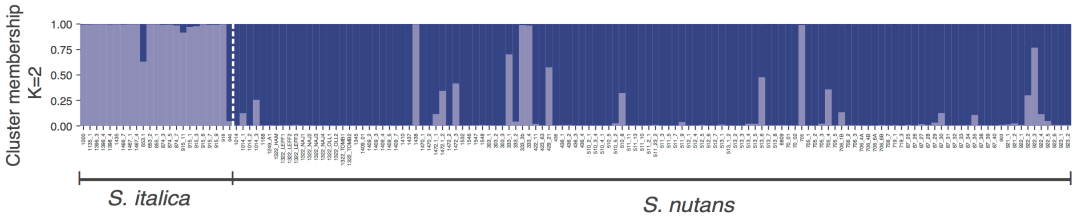

Fungal strains and their respective sampled host species

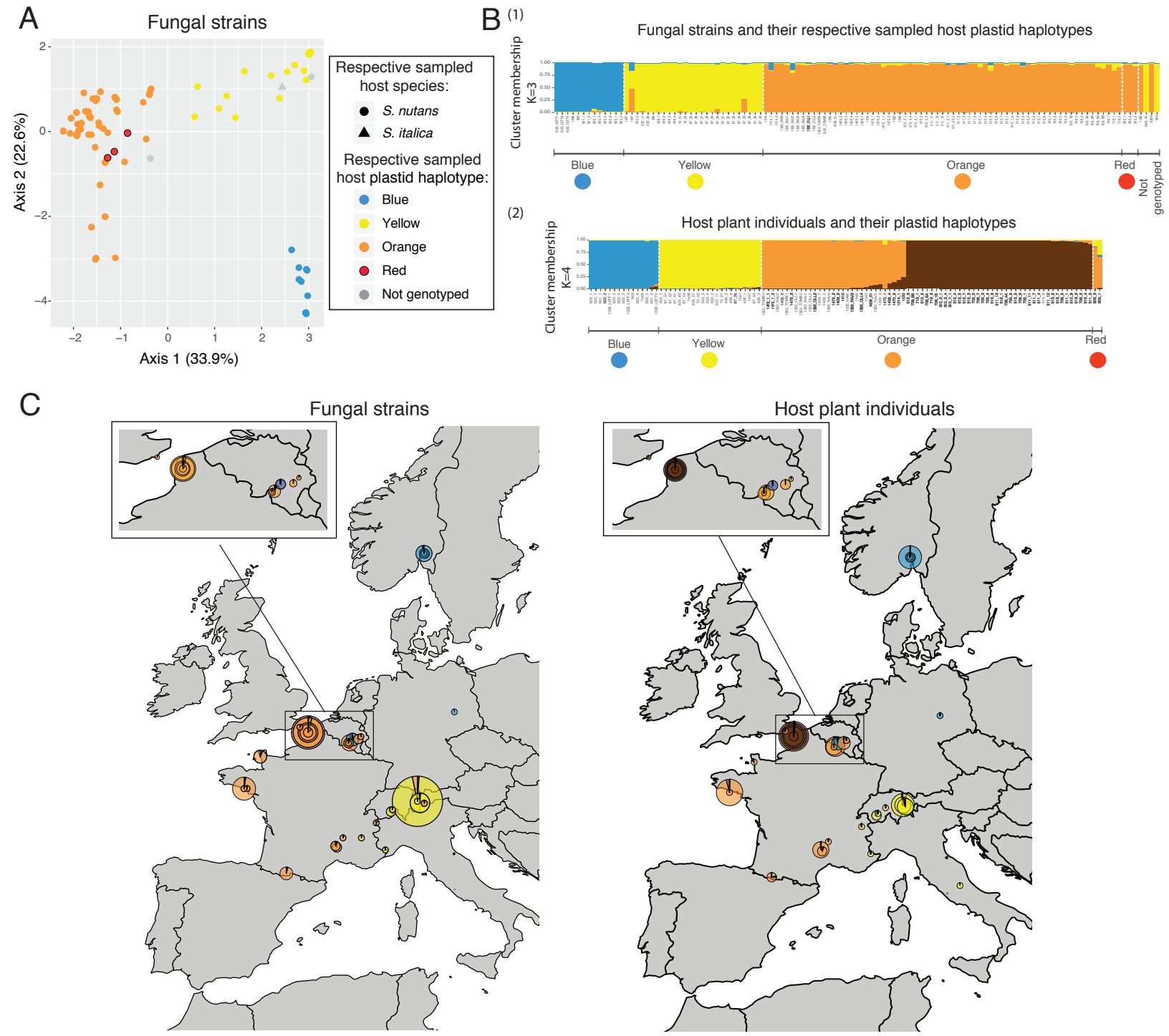
A
Fungal strains
Axis 2 (22.6%)
Axis 1 (33.9%)
Respective sampled host species:
S. nutans
S. italica
Respective sampled host plastid haplotype:
Blue
Yellow
Orange
Red
Not genotyped
B
(1)
Fungal strains and their respective sampled host plastid haplotypes
Cluster membership K=3
Blue
Yellow
Orange
Red
Not genotyped
(2)
Host plant individuals and their plastid haplotypes
Cluster membership K=4
Blue
Yellow
Orange
Red
C
Fungal strains
Host plant individuals

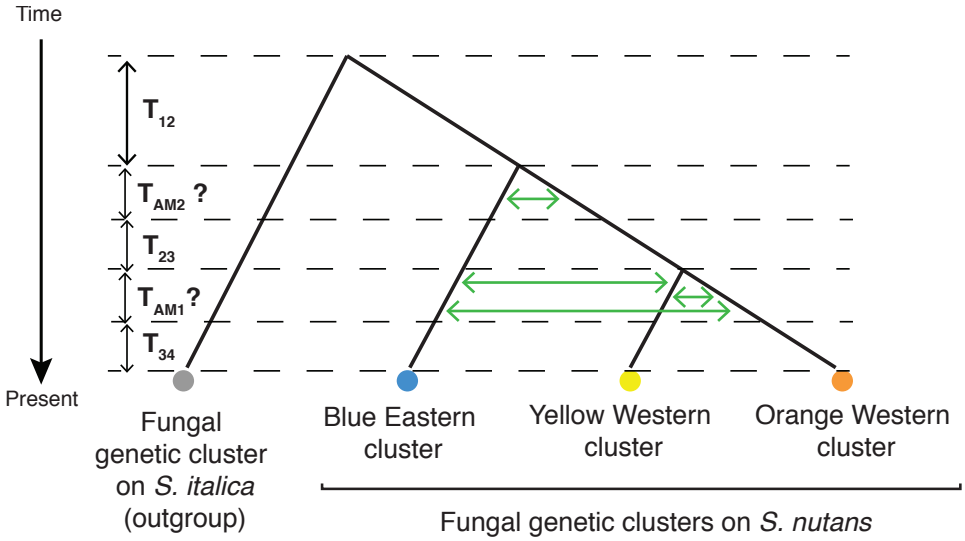
Time
Present
T_{12}
T_{AM2} ?
T_{23}
T_{AM1} ?
T_{34}
Fungal genetic cluster on *S. italica* (outgroup)
Blue Eastern cluster
Yellow Western cluster
Orange Western cluster
Fungal genetic clusters on *S. nutans*

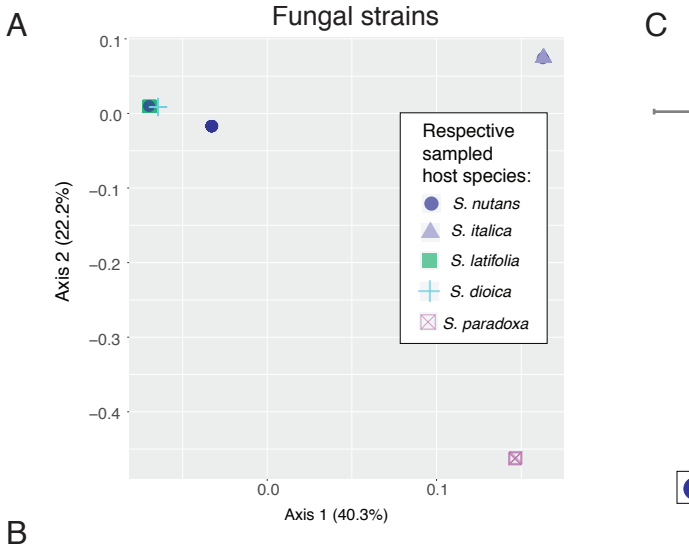
A
Fungal strains
Axis 2 (22.2%)
Axis 1 (40.3%)
0.1
0.0
−0.1
−0.2
−0.3
−0.4
0.0
0.1
Respective sampled host species:
S. nutans
S. italica
S. latifolia
S. dioica
S. paradoxa

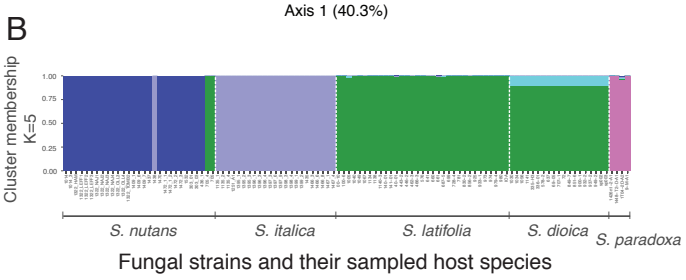
B
Cluster membership K=5
S. nutans
S. italica
S. latifolia
S. dioica
S. paradoxa
Fungal strains and their sampled host species

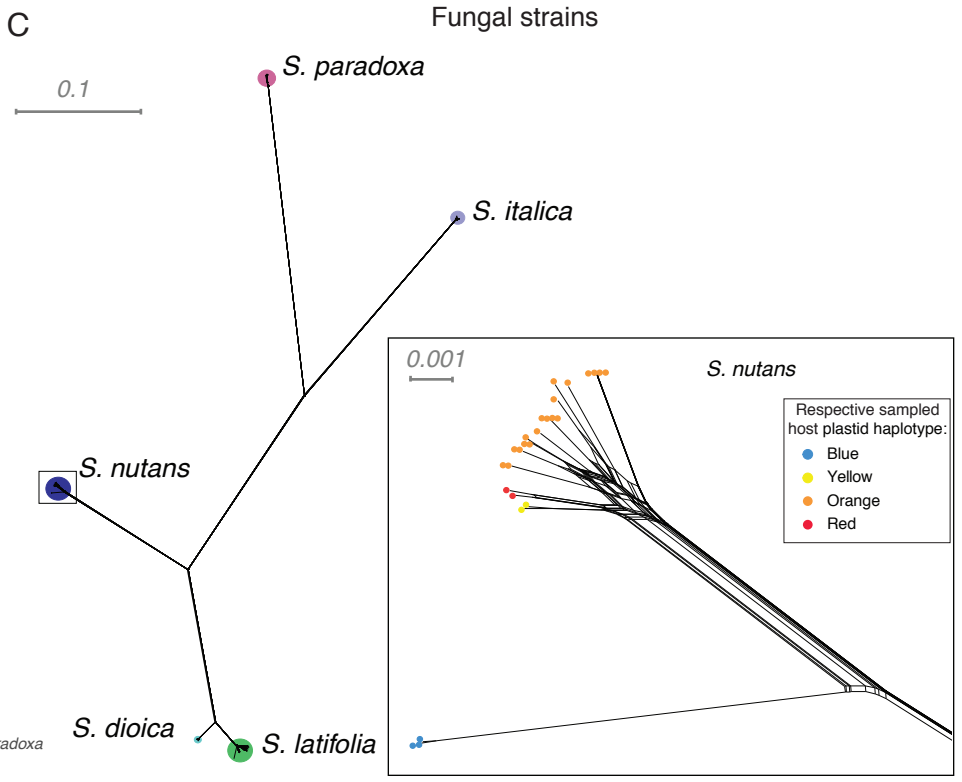
C
Fungal strains
0.1
S. paradoxa
S. italica
S. nutans
S. dioica
S. latifolia
0.001
S. nutans
Respective sampled host plastid haplotype:
Blue
Yellow
Orange
Red